THEMED ISSUE: Tectonics at the Micro- to Macroscale: Contributions in Honor of the University of Michigan Structure-Tectonics Research Group of Ben van der Pluijm and Rob Van der Voo

THE GEOLOGICAL SOCIETY OF AMERICA®

Vertical-axis rotations accommodated along the Mid-Cycladic lineament on Paros Island in the extensional heart of the Aegean orocline (Greece)

Christina Malandri[1], Konstantinos Soukis[2], Marco Maffione[1], Murat Özkaptan[3,*], Emmanuel Vassilakis[2], Stelios Lozios[2], and Douwe J.J. van Hinsbergen[1,†]

[1]DEPARTMENT OF EARTH SCIENCES, UNIVERSITY OF UTRECHT, BUDAPESTLAAN 4, 3584 CD UTRECHT, THE NETHERLANDS
[2]FACULTY OF GEOLOGY AND GEOENVIRONMENT, NATIONAL & KAPODISTRIAN UNIVERSITY OF ATHENS, GR-15784 ATHENS, GREECE
[3]DEPARTMENT OF GEOLOGICAL ENGINEERING, MIDDLE EAST TECHNICAL UNIVERSITY, 06531 ANKARA, TURKEY

ABSTRACT

The Aegean–west Anatolian orocline formed due to Neogene opposite rotations of its western and eastern limbs during opening of the Aegean back-arc basin. Stretching lineations in exhumed metamorphic complexes in this basin mimic the regional vertical-axis rotation patterns and suggest that the oppositely rotating domains are sharply bounded along a Mid-Cycladic lineament, the tectonic nature of which is enigmatic. Some have proposed this lineament to be an extensional fault accommodating orogen-parallel extension, while others have considered it to be a transform fault. The island of Paros hosts the only exposure of the E- to NE-trending lineations characterizing the NW Cyclades and the N-trending lineations of the SE Cyclades. Here, we show new paleomagnetic results from isotropic, ca. 16 Ma granitoids that intruded both domains and demonstrate that the trend difference resulted from post–16 Ma ~90° clockwise and 10° counterclockwise rotation of the NW and SE blocks, respectively. We interpret the semiductile to brittle, low-angle, SE-dipping Elitas shear zone that accommodated this rotation difference to reflect the Mid-Cycladic lineament. We conclude a two-stage exhumation history for Paros that is consistent with regional Aegean reconstructions. Between ca. 23 and 16 Ma, the metamorphic rocks of Paros were exhumed from amphibolite-facies to greenschist-facies conditions along a top-to-the-N detachment. The Elitas shear zone then started to exhume the northwestern, clockwise-rotating domain from below the southeastern, counterclockwise rotating domain since 16 Ma. From this, we infer that the Mid-Cycladic lineament is an extensional shear zone, consistent with geometric predictions that Aegean oroclinal bending was accommodated by orogen-normal and orogen-parallel extension.

LITHOSPHERE; v. 9; no. 1; p. 78–99; GSA Data Repository Item 2016359 | Published online 15 December 2016 doi:10.1130/L575.1

INTRODUCTION

Many orogens across Earth display variable degrees of curvature. Such curvature can be inherited from preexisting structures, e.g., related to a former passive-margin configuration, or so-called primary arcs (or bends), or it can be the result of bending of an originally straight orogen (Weil and Sussman, 2004). This second type of curved orogen, known as an orocline (Carey, 1955), involves relative vertical-axis rotation of its limbs (e.g., Speranza et al., 1997; Weil and Sussman, 2004; Marshak, 1988; Maffione et al., 2009; Yonkee and Weil, 2010; Pastor-Galan et al., 2015).

Vertical-axis rotation of a limb of an orocline kinematically equates to lateral variations in strain, either contractional or extensional, or a combination of these (Fig. 1). As a result, the core of an orocline is normally intensely deformed. In the case of "contractional" oroclines, orogen-parallel shortening of forearc slivers may lead to buckling of a preexisting part of the fold-and-thrust belt, with strong shortening in the center of the orocline, e.g., in Alaska (Johnston, 2001), eastern Australia (Li et al., 2012), or Cantabria, Spain (Pastor-Galan et al., 2015; Weil, 2006). Extensional oroclines, such as in Calabria, Italy, or the Aegean region, Greece, on the other hand, are normally interpreted to result from laterally varying amounts of slab roll-back (e.g., van Hinsbergen et al., 2005b; Jolivet et al., 2015), and their geometry can only be acquired through combined orogen-normal and orogen-parallel extension (van Hinsbergen and Schmid, 2012).

Previous paleomagnetic data have clearly demonstrated that the orogenic curvature of the Aegean–west Anatolian region (Fig. 2) resulted at least partly from opposite vertical-axis rotations of its western and eastern limbs (Horner and Freeman, 1983; Kissel and Poisson, 1987; Kissel et al., 1987; Kissel and Laj, 1988), which are located in the forearc above the Aegean subduction zone. These data indicate that ~50° clockwise (cw) rotation of the western limb occurred largely between 15 and 8 Ma (van Hinsbergen et al., 2005b), and ~20° counterclockwise (ccw) rotation of the eastern limb was completed between 15 and 5 Ma (van Hinsbergen et al., 2010a, 2010b), while the Moesian platform forming the northern hinterland of the Aegean orocline underwent little rotation (van Hinsbergen et al., 2008).

The Aegean orocline is composed of a thin-skinned fold-and-thrust belt of upper-crustal nappes that were offscraped from subducted continental and oceanic lithosphere of the African-Adriatic plate and were accreted to the

*Current address: Department of Geophysical Engineering, Karadeniz Technical University, TR-61080 Trabzon, Turkey.
†Corresponding author: d.j.j.vanhinsbergen@uu.nl.

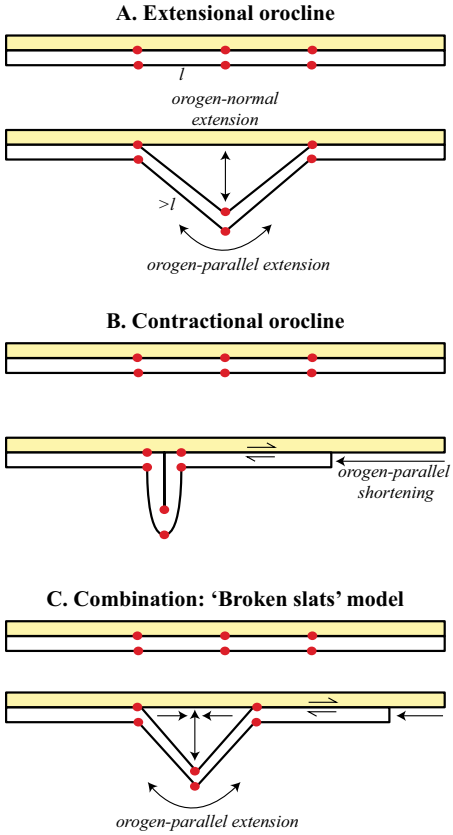

Figure 1. Styles of oroclinal bending. (A) In an extensional orocline, bending of the oroclinal limbs is accommodated by extension in the heart of the orocline, which must go hand in hand with orogen-parallel extension. (B) In a contractional orocline, the orogen buckles as a result of orogen-parallel shortening, whereby bending of the oroclinal limbs is not (necessarily) associated with orogen-parallel extension, but with contraction between the limbs. (C) A combination of both processes is frequently invoked for the Aegean region following the suggestion of Taymaz et al. (1991), whereby the oroclinal bending results from orogen-parallel convergence between western Greece and Anatolia, as well as orogen-normal extension interpreted to result from roll-back of the African slab below the Aegean region. In this case, both orogen-parallel extension in the outer limbs of the orocline, and orogen-parallel contraction in the core of the orocline are expected.

overriding Eurasian plate (van Hinsbergen et al., 2005a, 2010c; Jolivet and Brun, 2010). The center of the Aegean orocline, in the back arc, hosts a major extensional window that exposes deeply buried and metamorphosed parts of this fold-and-thrust belt that were exhumed along extensional detachments (Gautier et al., 1993; Sokoutis et al., 1993; Jolivet et al., 1996, 2010a; Lister et al., 1984; Tirel et al., 2009; Ring et al., 2010). Estimates of the maximum total amount of orogen-normal extension in the Aegean orocline are on the order of 400 km (Gautier et al., 1999; Jolivet and Brun, 2010; van Hinsbergen and Schmid, 2012).

Today, general agreement exists that the trench-normal extension in the heart of the Aegean orocline is kinematically linked to the oroclinal bending of the forearc limbs (Brun and Sokoutis, 2007, 2010; van Hinsbergen and Schmid, 2012; Jolivet et al., 2015; Menant et al., 2016). The clearest direct link between extension and rotation is provided in two triangular extensional complexes in the Rhodope mountains of northern Greece, and in the Menderes Massif of western Turkey (Fig. 2). There, stretching lineations associated with Miocene extensional detachments display a change in azimuth over an angle that is proportional to the triangular shape of the extensional complex, and that coincides with the paleomagnetically determined vertical-axis rotation difference across the extensional complexes (Brun and Sokoutis, 2007; van Hinsbergen et al., 2010b). The change in azimuth of stretching lineations in metamorphic rocks exposed across the Aegean extensional windows was already noted by Walcott and White (1998), and kinematic reconstructions have since used these lineations as markers for the amount of rotation of the crystalline bodies exposed in the center of the orocline (Brun and Sokoutis, 2010; van Hinsbergen and Schmid, 2012; Menant et al., 2016). A recent quantitative orocline test confirmed the proportionality of the paleomagnetically determined vertical-axis rotation and the azimuth of stretching lineations across the Aegean–west Anatolian region (Pastor-Galán et al., 2016).

Despite this agreement, there is fierce debate on the mechanisms that produced such variation of stretching lineation orientations across the Aegean orocline. This debate is centered on the observation of Walcott and White (1998) that the stretching lineations in Greece abruptly change orientation across a narrow zone, known as the Mid-Cycladic lineament, in the Cycladic metamorphic complex (Fig. 2). Lineations to the north of this lineament trend approximately ENE-WSW to NE-SW, e.g., associated with the North Cycladic detachment (Fig. 2; Jolivet et al., 2010a), whereas those to the south, e.g., on Naxos, trend approximately N-S. Walcott and White (1998) tentatively suggested that the Mid-Cycladic lineament may reflect a strike-slip fault zone (Fig. 2).

Two end-member scenarios were proposed for the restoration of opposite rotations in the Aegean orocline. On the one hand, van Hinsbergen and Schmid (2012) pointed out that the formation of an extensional orocline geometrically requires not only orogen-normal, but also orogen-parallel extension, increasing in magnitude from the hinterland toward the trench (Fig. 1). Such multidirectional extension, leading to strong crustal attenuation, was nicely portrayed in analogue models of gravitational spreading (Gautier et al., 1999). However, where the analogue models of Gautier et al. (1999) displayed regionally distributed orogen-parallel extension alongside orogen-normal extension, the abrupt change of stretching lineations across the Mid-Cycladic lineament was interpreted by van Hinsbergen and Schmid (2012) as a reflection of localization of the orogen-parallel extension along a single regional structure, which they conceptually termed the Mid-Cycladic detachment. In their reconstruction, van Hinsbergen and Schmid (2012) restored the SE Cycladic massifs, with approximately N-S stretching lineations, below the NW Cycladic massifs that display ENE-WSW stretching lineations, and restored both to their inferred original NNE-SSW orientation. Others, including Jolivet et al. (2013, 2015), Philippon et al. (2014), Menant et al. (2016), and Brun et al. (2016), have cited the absence of field evidence for such a major detachment and instead proposed a restoration in which the two domains were originally located next to each other prior to rotation. Their models, reminiscent of the "broken slats" model of Taymaz et al. (1991), instead argue for major orogen-parallel contraction generating orogen-normal extension (Fig. 1). Where Taymaz et al. (1991) pointed at the North Anatolian fault zone, along which Anatolia moves westwards toward the Aegean region, as evidence for orogen-parallel shortening, the total amount of orogen-parallel shortening required in the restorations of Jolivet et al. (2013, 2015), Philippon et al. (2014), Menant et al. (2016), and Brun et al. (2016) of at least 300 km well exceeds the estimated displacement along the North Anatolian fault zone of only 60–85 km (Şengör et al., 2005; Hubert-Ferrari et al., 2002; Le Pichon et al., 2016), of which some 50 km occurred after 2.5 Ma (Hubert-Ferrari et al., 2009), i.e., after the bulk of the bending of the Aegean orocline. The absence of any evidence of orogen-parallel strike-slip displacements of hundreds of kilometers in either northern Turkey, or between northwestern Greece or Albania and the Moesian platform, is one of the key arguments of van Hinsbergen and Schmid (2012) to infer major orogen-parallel extension in their model.

As mentioned, the Cycladic island of Paros (Fig. 2) is the only location where the abrupt change in stretching lineations characteristic for both sides of the Mid-Cycladic lineament is exposed; approximately E-W stretching lineations pertain in the north, and approximately N-S lineations do so in the south (Gautier et al., 1993; Walcott and White, 1998). The metamorphic rocks that contain these stretching

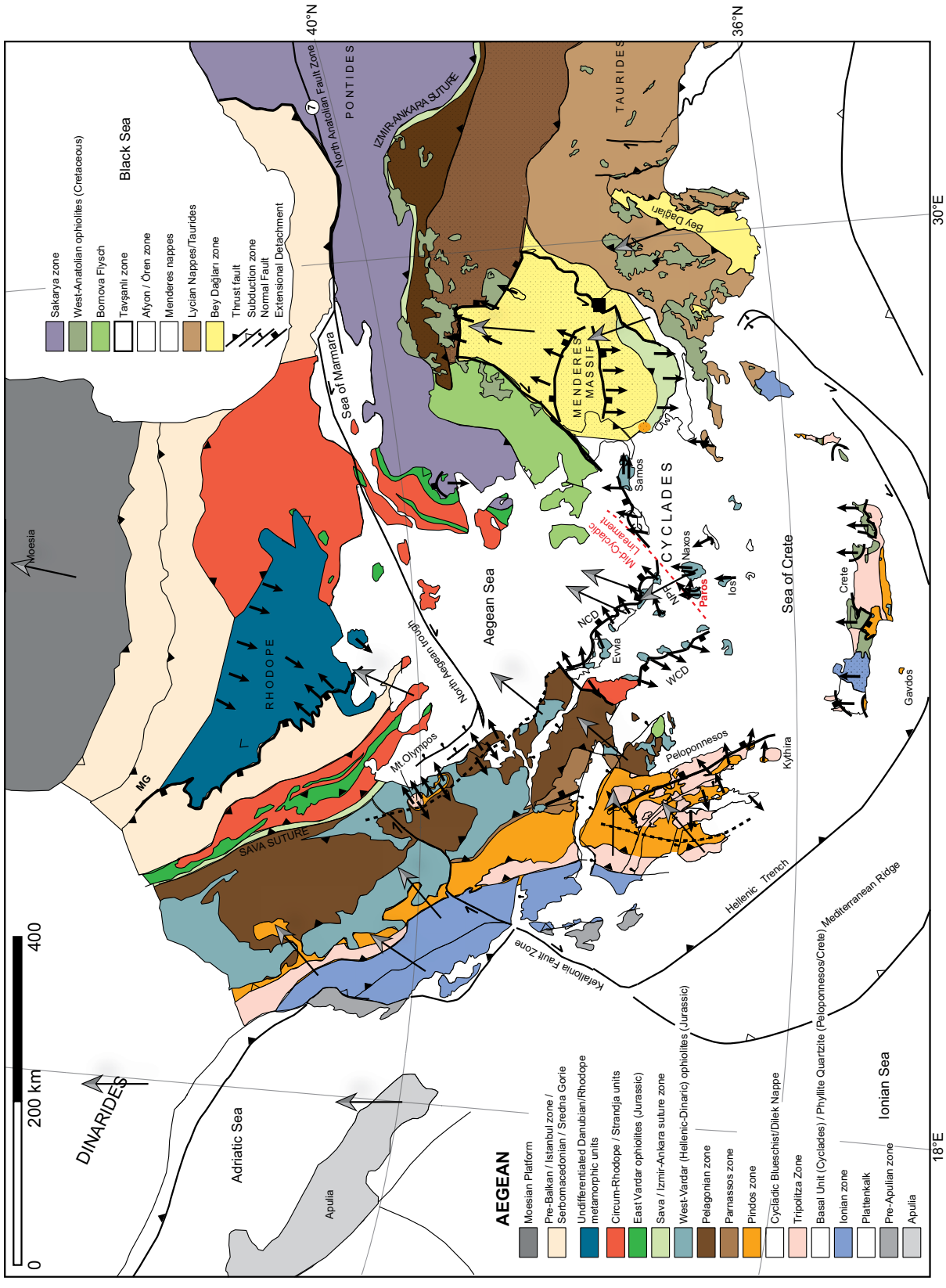

Figure 2. Tectonic map of the Aegean–west Anatolian region, modified after van Hinsbergen and Schmid (2012). Stretching lineation directions are from Hetzel et al. (1995), Walcott and White (1998), Bozkurt and Satir (2000), Okay (2001), Işık and Tekeli (2001), Lips et al. (2001), Işık et al. (2003, 2004), Rimmelé et al. (2003), Ring et al. (2003), Brun and Sokoutis (2007), Rosenbaum et al. (2007), Marsellos and Kidd (2008), Cavazza et al. (2009), Diamantopoulos et al. (2009), Tirel et al. (2009), van Hinsbergen and Boekhout (2009), Jolivet et al. (2010b, 2015), Ring et al. (2011), and Grasemann et al. (2012). Paleomagnetic declinations were compiled from Horner and Freeman (1982, 1983), Kissel et al. (1984, 1985, 1989, 1995), Kissel and Poisson (1987), Kissel and Laj (1988), Speranza et al. (1992, 1995), Morris and Robertson (1993), Mauritsch et al. (1995, 1996), Morris (1995), Morris and Anderson (1996), van Hinsbergen et al. (2005b, 2008, 2010a, 2010b, 2014), and de Leeuw et al. (2012). Map shows the regional pattern of stretching lineations and paleomagnetic declinations from Oligocene to Lower Miocene rocks. ECD—East Cycladic detachment system, NCD—North Cycladic detachment system, NPF—Naxos-Paros fault system, WCD—West Cycladic detachment system.

lineations have been intruded by Miocene granitoid bodies and rhyolitic dikes (ca. 16 Ma and ca. 7 Ma, respectively; Bargnesi et al., 2013) that do not show field evidence for ductile deformation. Here, we present paleomagnetic and anisotropy of magnetic susceptibility (AMS) analyses from these granitoids to test whether the observed variation in the orientation of the lineations on Paros Island is caused by relative vertical-axis rotation of distinct crustal domains. We will evaluate the structure that bounds the two domains and discuss whether any rotation differences found may result from strike-slip, thrusting, or extension. We will then use the tectonic history of Paros Island to discuss the regional importance of the Mid-Cycladic lineament in accommodating opposite rotations, and evaluate the extent to which these rotations may have influenced the thermal regime in the heart of the Aegean orocline.

GEOLOGICAL SETTING

Aegean Region

The Aegean orocline (Fig. 2) was broadly formed in two stages. The first stage included Late Jurassic to Paleogene subduction, and stacking of nappes derived from Gondwana-derived continental blocks and from intervening deep-marine, partly oceanic basins to the southern Eurasian margin (van Hinsbergen et al., 2005a, 2010c; Jolivet and Brun, 2010). In a second stage, ongoing accretion was accompanied by extension of the previously accreted and thickened crust in a back-arc setting through crustal-scale detachments that were accompanied by widespread plutonism and volcanism, since Eocene–Oligocene time (Fytikas et al., 1984; Lister et al., 1984; Gautier and Brun, 1994; Gautier et al., 1999; Jolivet, 2001; Keay et al., 2001; Brun and Faccenna, 2008; Tirel et al., 2009; Jolivet et al., 2010a; Jolivet and Brun, 2010; Ring et al., 2010; Grasemann et al., 2012; Soukis and Stockli, 2013). This extension is attributed to southward retreat of the subduction zone relative to Eurasia, normally interpreted to reflect slab roll-back (Le Pichon and Angelier, 1981; Royden, 1993; Jolivet and Brun, 2010), and it resulted in thinning of the crust to ~26–22 km in and around the Cycladic massif (Tirel et al., 2004). Extension of the Cycladic domain exhumed deeply buried rocks from underneath a hanging wall that consists of low-grade or nonmetamorphic continental nappes as well as ophiolites. These hanging-wall rocks are represented by extensional klippen (Durr et al., 1978; Jolivet and Brun, 2010; Jolivet et al., 2010a; Ring et al., 2010).

In the Cycladic domain (central Aegean region), four major tectonic units have been recognized. The highest structural unit is the Upper Cycladic nappe. The Upper Cycladic nappe is a highly heterogeneous, dismembered group of rocks consisting of nonmetamorphosed Upper Paleozoic to Mesozoic sediments correlated to the Pelagonian zone and ophiolitic rocks associated with greenschist- to amphibolite-facies metamorphic metabasalts and metasediments with no evidence of high-pressure (HP) metamorphism that are intruded by Upper Cretaceous granitoids (Durr et al., 1978; Altherr et al., 1982; Papanikolaou, 1987; Avigad and Garfunkel, 1991; Bröcker and Franz, 2006; Jolivet and Brun, 2010; Ring et al., 2010; Bargnesi et al., 2013). These rocks are found as isolated klippen in the hanging wall of the detachments, and are in several places overlain by Upper Miocene clastic sediments deposited in a supradetachment basin (Durr et al., 1978; Bögek, 1983; Sánchez-Gómez et al., 2002; Jolivet and Brun, 2010; Ring et al., 2010; Bargnesi et al., 2013).

The dominant tectonic unit with widespread exposure on the Cyclades is the Cycladic Blueschist Unit, a composite rock association consisting of Mesozoic metabasic and meta-acidic rocks intercalated within schists and marbles (Durr et al., 1978; Blake et al., 1981; Altherr et al., 1982; Avigad and Garfunkel, 1991; Bröcker and Pidgeon, 2007). The Cycladic Blueschist Unit is generally considered as the lateral equivalent of the Pindos zone in the Hellenides (Fig. 2; Bonneau, 1982; van Hinsbergen et al., 2005c). It is underlain by pre-Alpine basement consisting of paragneisses and orthogneisses (Andriessen et al., 1987; Engel and Reischmann, 1998; Keay et al., 2001; Bargnesi et al., 2013). The nature of the contact between the Cycladic Blueschist Unit and the pre-Alpine basement is debated, with some researchers suggesting that it represents a detachment (Forster and Lister, 1999; Thomson et al., 2009), while others argue it is a thrust (Huet et al., 2009).

In a few places, for example, Evvia and Samos Islands and Mount Olympos (Fig. 2), the Basal Unit is exposed, consisting of Mesozoic to Eocene neritic carbonates with an Upper Eocene–Oligocene flysch (Ring et al., 2001, 2007a, 2007b). The Basal Unit tectonically underlies the Cycladic Blueschist Unit, but its relation to the pre-Alpine basement is unclear. The Basal Unit correlates to the nonmetamorphic Gavrovo-Tripolitza unit exposed in the Aegean forearc (Fig. 2; Kisch, 1981; Ring et al., 2001; van Hinsbergen et al., 2005c).

The Cycladic islands are characterized by a complex metamorphic evolution. The Cycladic Blueschist Unit and the Basal Unit experienced Early Eocene and Late Oligocene–Early Miocene subduction down to high-pressure–low-temperature (HP-LT) conditions, respectively. For the Cycladic Blueschist Unit, the HP event is dated between 55 and 40 Ma (Wijbrans et al., 1990; Bröcker et al., 1993; Bröcker and Franz, 1998, 2006), although in Evia and Sifnos, much younger ages of 30–33 Ma were reported by Ring et al. (2007a, 2011). The Cycladic Blueschist Unit experienced peak metamorphic conditions in the stability field of blueschist and eclogite reaching locally up to 15–20 kbar and 550 °C (Schliestedt and Matthews, 1987; Okrusch and Bröcker, 1990). This event was followed by a greenschist-facies overprint in the Late Oligocene–Miocene with pressure-temperature (*P-T*) conditions at ~450–500 °C and 4–9 kbar (Altherr et al., 1982; Schliestedt and Matthews, 1987; Okrusch and Bröcker, 1990; Bröcker et al., 1993; Bröcker and Franz, 1998). In the central Cyclades, on Paros and Naxos, the Late Oligocene–Early Miocene event was associated with significant heating and granitoid intrusion, and it reached amphibolitic to granulitic conditions, resulting occasionally in partial melting and formation of migmatitic bodies (Jansen and Schuiling, 1976; Buick and Holland, 1989; Jolivet et al., 2015). Since latest Oligocene time, the Cycladic Blueschist Unit and deeper units have been exhumed by crustal-scale detachment systems, summarized as the North Cycladic detachment system, the West (or South) Cycladic detachment system, and the Naxos-Paros fault system (Gautier et al., 1993; Brichau et al., 2006; Tirel et al., 2009; Jolivet et al., 2010a; Iglseder et al., 2011; Ring et al., 2011; Grasemann et al., 2012). In the mid- to Late Miocene, the magmatic arc migrated southward, producing syn- to postextensional granitoids that cut the regional foliation and, in many cases, are deformed by the extensional detachments (Durr et al., 1978; Altherr et al., 1982; Bolhar et al., 2010, 2012; Ring et al., 2010; Grasemann et al., 2012; Bargnesi et al., 2013; Jolivet et al., 2015; Menant et al., 2016).

Geology of Paros Island

The island of Paros lies within the Cycladic metamorphic complex in the central part of the Aegean Sea (Fig. 2), and it is composed of four lithostratigraphic units with complex tectonostratigraphic histories, likely owing to Miocene extension (Papanikolaou, 1977, 1980; Robert, 1982; Gautier et al., 1993; Brichau et al., 2006; Bargnesi et al., 2013). These are, from top to bottom, the Marmara, Dryos, Marathi, and pre-Alpine basement units (Fig. 3).

Marmara Unit

The Marmara Unit is the upper tectonostratigraphic unit of the island and prevalently crops out in the northeast part of the island. It is

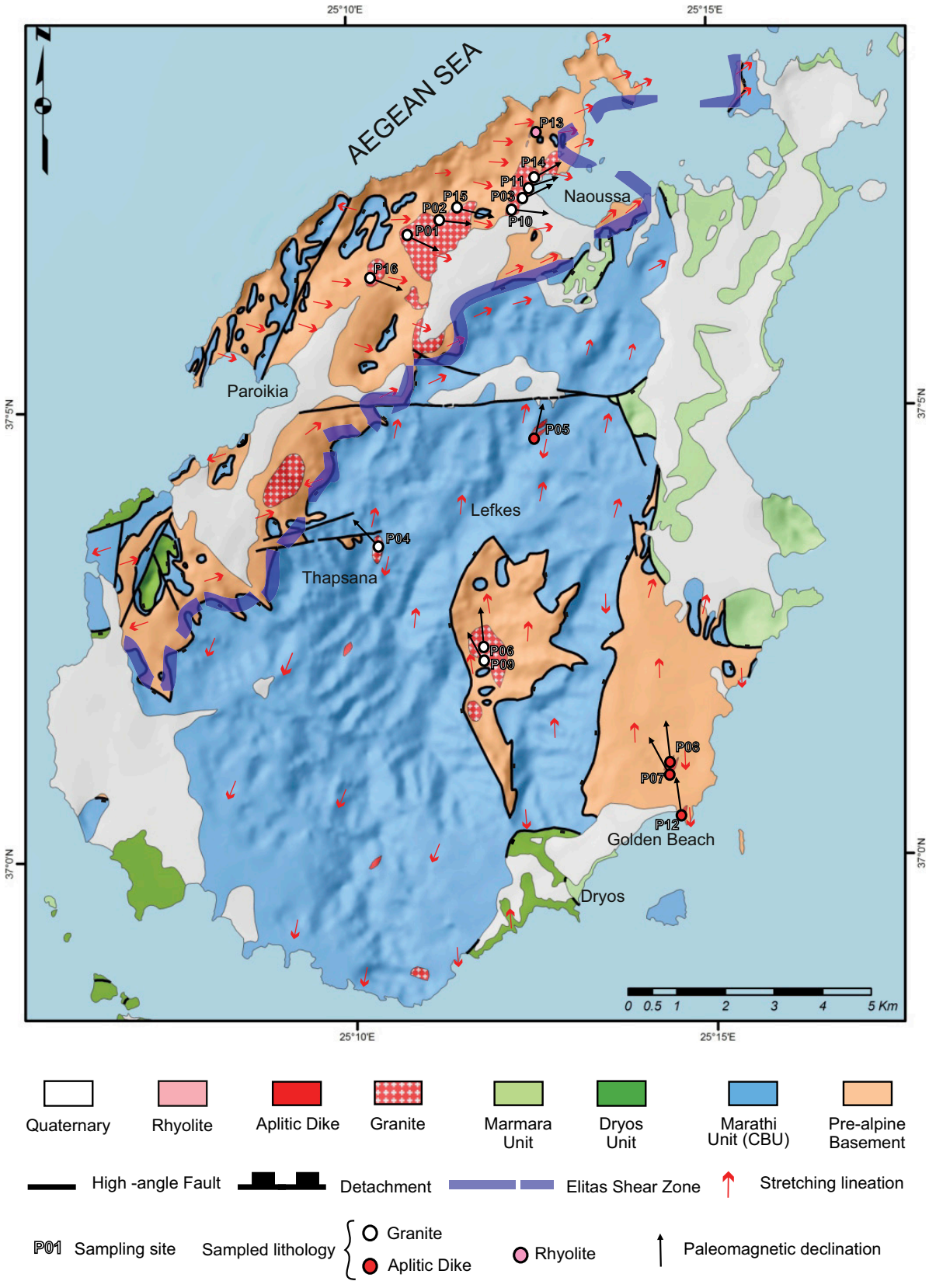

Figure 3. Geological map of Paros Island with sampling locations (modified after Papanikolaou 1996), and stretching lineation measurements (this study). CBU—Cycladic Blueschist Unit.

juxtaposed against the underlying Marathi and pre-Alpine basement units by a detachment fault (Piso Livadi detachment) that is located at the base of the Marmara Unit (Fig. 4A). The Piso Livadi detachment is a ductile-to-brittle, low-angle normal fault observed only on the eastern-northeastern part of the island. Shear sense indicators in the footwall ultramylonitic orthogneiss and striations on the fault surface (Fig. 4B; 37°02′28.22″N, 25°15′47.26″E) show in general a top-to-the-N sense of shear. The hanging-wall Marmara Unit consists of serpentinized peridotites, clastic sedimentary formations and Cretaceous limestones, and Miocene conglomerates, sandstones, and sandy marls. The Miocene sediments are interpreted as a supradetachment basin fill that starts with Lower Miocene marine sediments shifting gradually to continental environment deposition toward the Upper Miocene strata (Sánchez-Gómez et al., 2002; Bargnesi et al., 2013). Recent analysis suggested that the Cretaceous limestones and ophiolitic rocks are allochthonous olistoliths that were redeposited into the supradetachment basin (Bargnesi et al., 2013). These sediments often present slumping structures (Fig. 4C; 37°02′34.04″N, 25°15′56.42″E), and they are intensely deformed with faults and folds associated with synextensional sedimentation and slip along the Piso Livadi detachment.

Dryos Unit

The Dryos Unit overlies the Marathi Unit and is characterized by limited exposure along the southeastern and southwestern coast (Fig. 3). It is a heterogeneous unit consisting of metabasites, meta-calcareous rocks, phyllites, and schists as the main lithologies. Based on index minerals in metabasites and schists (e.g., chlorite, actinolite, epidote, and albite), the Dryos Unit underwent low- to medium-grade metamorphism, up to greenschist facies (Robert, 1982; this study). The rocks are normally highly schistose and often crenulated with NNW-SSE tight to isoclinal recumbent folds that produced an axial planar cleavage. Late-stage brittle deformation produced block tilting and rotation of the rocks, which now appear to have a vertical foliation (SE Paros; 36°59′29.57″N, 25°13′8.04″E). In some places close to the contact with Marathi Unit, a well-developed mylonitic fabric is present (SE Paros; 37°00′16.03″N, 25°12′36.71″E). In general, the contact with the underlying Marathi Unit is accompanied by a thick cataclastic fault zone, in which shear sense indicators such as shear bands, rotated clasts, asymmetric folds, and Riedel-shears (Fig. 4D; 36°59′30.88″N, 25°13′09.88″E) indicate top-to-the-S sense of shear for the late-stage brittle part of the history. In a few places, though, for example, within the mylonitic rocks near the village of Dryos (SE Paros Island), δ-clasts, S-C′ fabric, and flanking folds indicate top-to-the-N sense of shear for the brittle-ductile event (Fig. 4E; 37°00′16.03″N, 25°12′36.71″E). Based on (U-Th)/He thermochronometry, Bargnesi et al. (2013) showed that the Dryos Unit and the underlying Marathi Unit in the central-south parts were exhumed through the zircon and apatite helium partial retention zone (~180–40 °C) together in the footwall of the Piso Livadi detachment after 11–10 Ma.

Marathi Unit

The Marathi Unit occupies most of the central part of the island (Fig. 3), and it is considered to be the Cycladic Blueschist Unit, but overprinted by amphibolite- to granulite-facied metamorphism (Robert, 1982; Gautier et al., 1993; Bargnesi et al., 2013). Contrary to Naxos Island, no HP mineral assemblage is yet reported from Paros. The lithologies on Paros include amphibolites, amphibolitic schists intercalated with thin layers of impure marbles, metabauxite-bearing marbles, quartzofeldspathic rocks, and mica schists. These lithologies are intensely folded and underwent at least three successive refolding events on a macroscopic scale (Fig. 4F; south of Naoussa, 37°06′06.26″N, 25°13′46.03″E; Aghios [Ag]. Georgios Monastery 37°1′22.39″N, 25°12′47.76″E; Papanikolaou, 1980). Robert (1982) identified a metamorphic gradient from the gneiss dome in the center of the island, which contains the highest metamorphic grade, toward the south (including the Dryos Unit) and distinguished three zones with mineral assemblages ranging from upper amphibolite facies in the center of the dome to lower amphibolite and finally to greenschist facies in the south. At the base of the unit, usually along the contact with the pre-Alpine basement, the rocks of the Marathi Unit present a mylonitic to ultramylonitic fabric with a few meters thickness, which is variably overprinted by cataclastic deformation that produced thick proto- to ultracataclasites (Fig. 4G; 37°6′59.43″N, 25°10′0.69″E, and in Naoussa 37°7′34.14″N, 25°14′35.81″E).

Pre-Alpine Basement

The pre-Alpine basement is largely made of variably deformed orthogneisses corresponding to a granitic protolith of Variscan age (325–302 Ma; Engel and Reischmann, 1998). In many areas, the mineral composition in the orthogneisses includes alkali-feldspars, plagioclase, quartz, biotite, white micas, and opaques. The orthogneisses are characterized by a gneissic foliation, formed by alternating dark- and light-colored layers, which is variably transposed by subsequent mylonitization. In many places below the Marathi Unit, the orthogneisses have become a mylonite (Fig. 4H; 37°7′54.52″N, 25°12′48.04″E) or an L-tectonite (e.g., eastern Paros, north of the village of Piso Livadi; Fig. 4I; 37°2′20.25″N, 25°15′41.24″E), interpreted as a result of the Miocene detachment faulting.

The orthogneisses are intruded by Middle Miocene (ca. 16 Ma, laser ablation–inductively coupled plasma–mass spectrometry [LA-ICP-MS] zircon U-Pb dating; Bargnesi et al., 2013), almost undeformed, S-type two-mica granites (Fig. 3; Altherr et al., 1982; Stouraiti et al., 2010). At the northern part of the island, numerous granitic intrusions are observed between Paroikia and Naoussa. In this area, the roof of the granites is situated ~50–100 m below the basement–Cycladic Blueschist Unit contact (Fig. 4J; south of Kolympithres, 37°7′35.77″N, 25°12′32.70″E), whereas at the central and southern parts the granites pierce through this contact (e.g., near Thapsana; Fig. 4K; 37°3′31.99″N, 25°10′27.60″E). In the central part, the granites are spatially associated with the migmatitic dome (Fig. 4L; 37°2′19.47″N, 25°11′59.01″E). Numerous aplitic and pegmatitic dikes can be observed near the granitic intrusions, especially in the northernmost part of the island. They are variably deformed, ranging from almost vertical and undeformed (Fig. 4M; 37°4′53.18″N, 25°12′43.47″E) to slightly schistose, to completely parallel with the foliation of the host orthogneisses, in which case they are isoclinally folded and/or boudinaged (see following section). The youngest intrusive rocks are some rhyolitic dikes observed at the northern part of the island. These rocks have intruded along N-S fractures (e.g., approximately perpendicular to the local trend of the stretching lineation), and they are undeformed (Fig. 4N; 37°8′19.88″N, 25°12′40.98″E). According to LA-ICP-MS zircon U-Pb dating and (U-Th)/He thermochronometry by Bargnesi et al. (2013), the age of the dikes is 7–8 Ma.

STRUCTURAL OBSERVATIONS

Detailed structural investigations were carried out mostly on the northern part of the island to identify the structure related to the change in the trend of the stretching lineation seen in the foliation of the metamorphic rocks. The stretching lineation trends approximately E-W in the north and northwestern part of the island (Fig. 5A) and approximately N-S in the central and southeastern part (Fig. 5B). Our study revealed a regional NNE-SSW–striking, ESE-dipping shear zone associated with a succession of structures evolving in the footwall from ductile to semiductile to brittle conditions, and

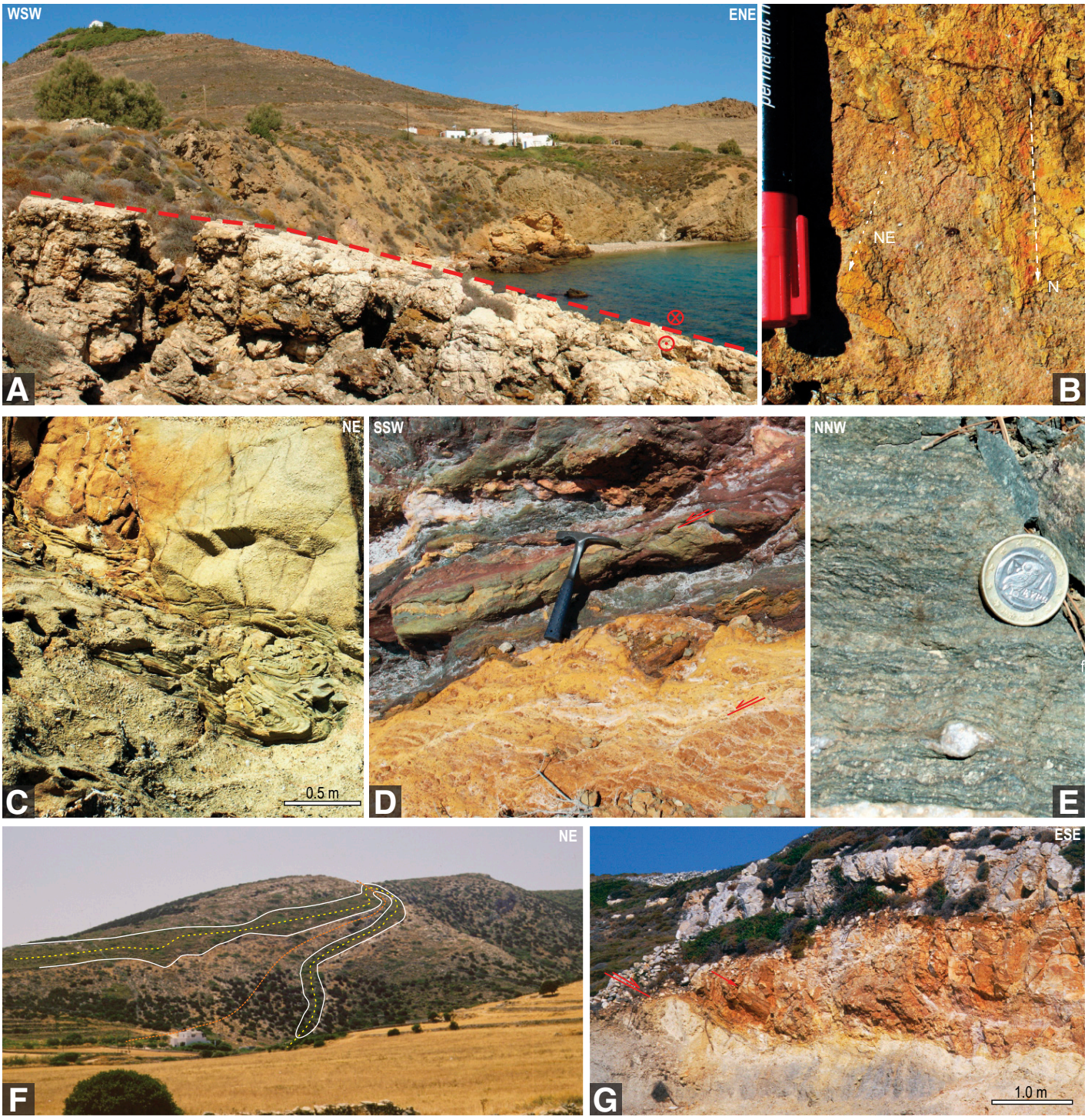

Figure 4. (A) View of the Piso Livadi detachment, which juxtaposes Neogene sediments of the Marmara Unit (hanging wall) against dolomitic marble of the Marathi Unit (footwall). (B) Detail of the fault surface with N and NE slickenlines. (C) Upper Miocene clastic sediments above the supradetachment with slump structures in the intermediate fine-grained layers. (D) Cohesive cataclasites cut by SSW-dipping Riedel shears and brittle shear zones (see arrows) indicating top-to-SSW sense of shear for the brittle stage of the deformation at the contact between the Dryos and Marmara Units near Dryos Village. (E) Quartzitic δ-clast indicating top-to-the-N sense of shear in the mylonitized metabasic rocks of Dryos Unit north of the village of Dryos. (F) Refolded folds in Marathi Unit (north Paros), where at least two axial plane traces can be identified. (G) View of the contact between the overlying marbles of the Marathi Unit and the underlying orthogneiss (gray) north of Paroikia. The contact is a 3–5-m-thick E-dipping cataclastic fault zone where the marbles are strongly brecciated and infiltrated by fluids. Secondary brittle faults have E-dipping striations (arrow). The roof of the orthogneiss is a white clayish ultracataclasite with aligned clasts deriving from the orthogneiss. (*Continued on following page.*)

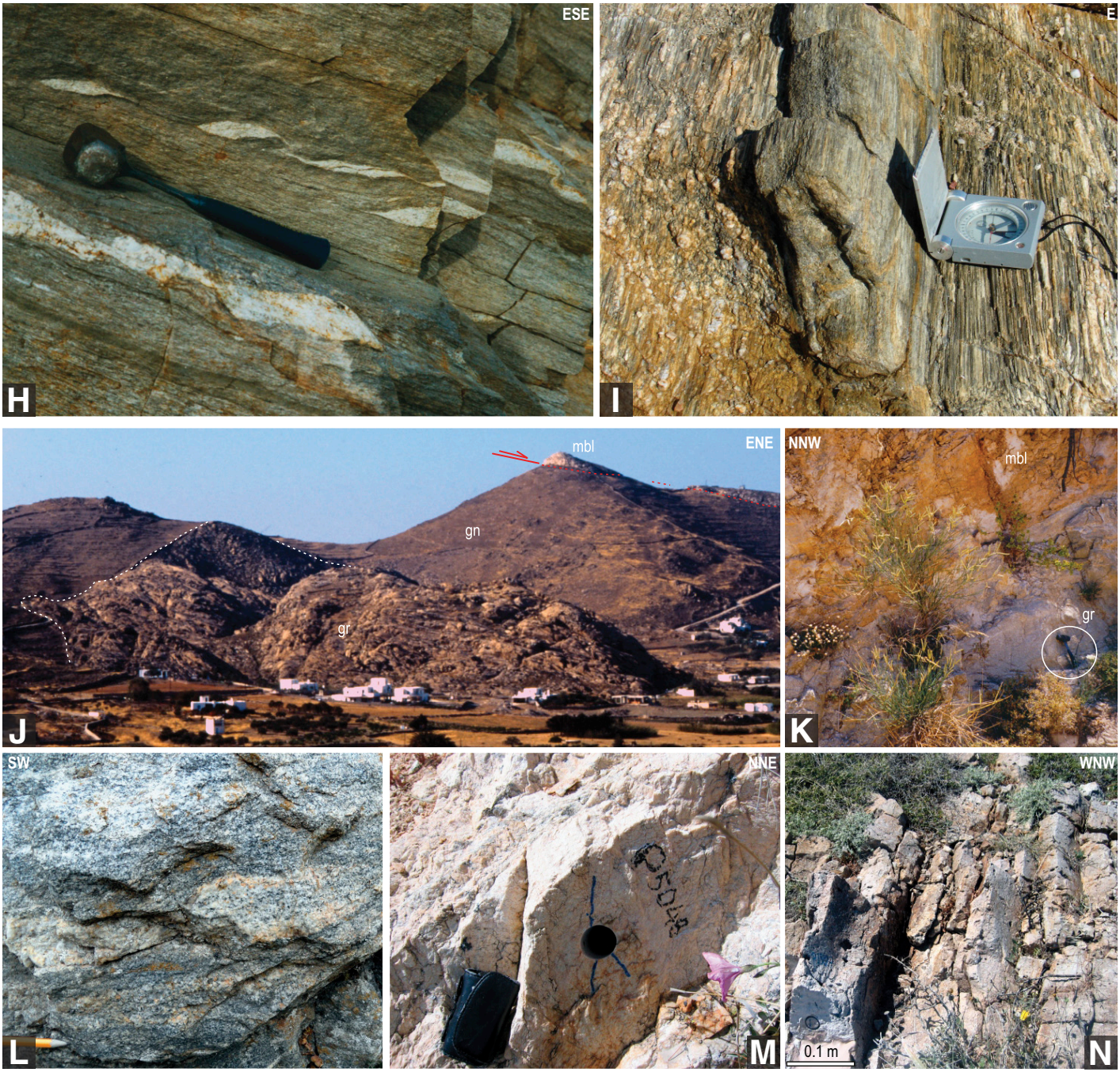

Figure 4 (*continued*). (H) Rotated boudinaged aplitic vein in the mylonitic orthogneisses of northern Paros with sense of shear top-to-the-ESE. (I) L-tectonite orthogneiss in the footwall of the Piso Livadi detachment. (J) View of the Kolympithres granite (gr), which has intruded into the basement orthogneiss below the E-dipping contact with the Marathi marble (mbl). gn—gneiss. (K) Sharp intrusive contact between fluid-infiltrated yellow to light-brown Marathi marbles (mbl) and Middle Miocene granite (gr) in Thapsana. The contact is probably reactivated, since limited brecciation can be observed locally in both lithologies. (L) Close-up view of the sampled undeformed granitic rocks near the center of the migmatitic dome. (M) Aplitic dike near Kostos village. These are late-stage dikes that cut through the foliation, and they are completely undeformed. (N) Close-up view of the undeformed Upper Miocene rhyolitic dikes that have intruded the orthogneiss at the northern part of the island, along approximately N-S fractures.

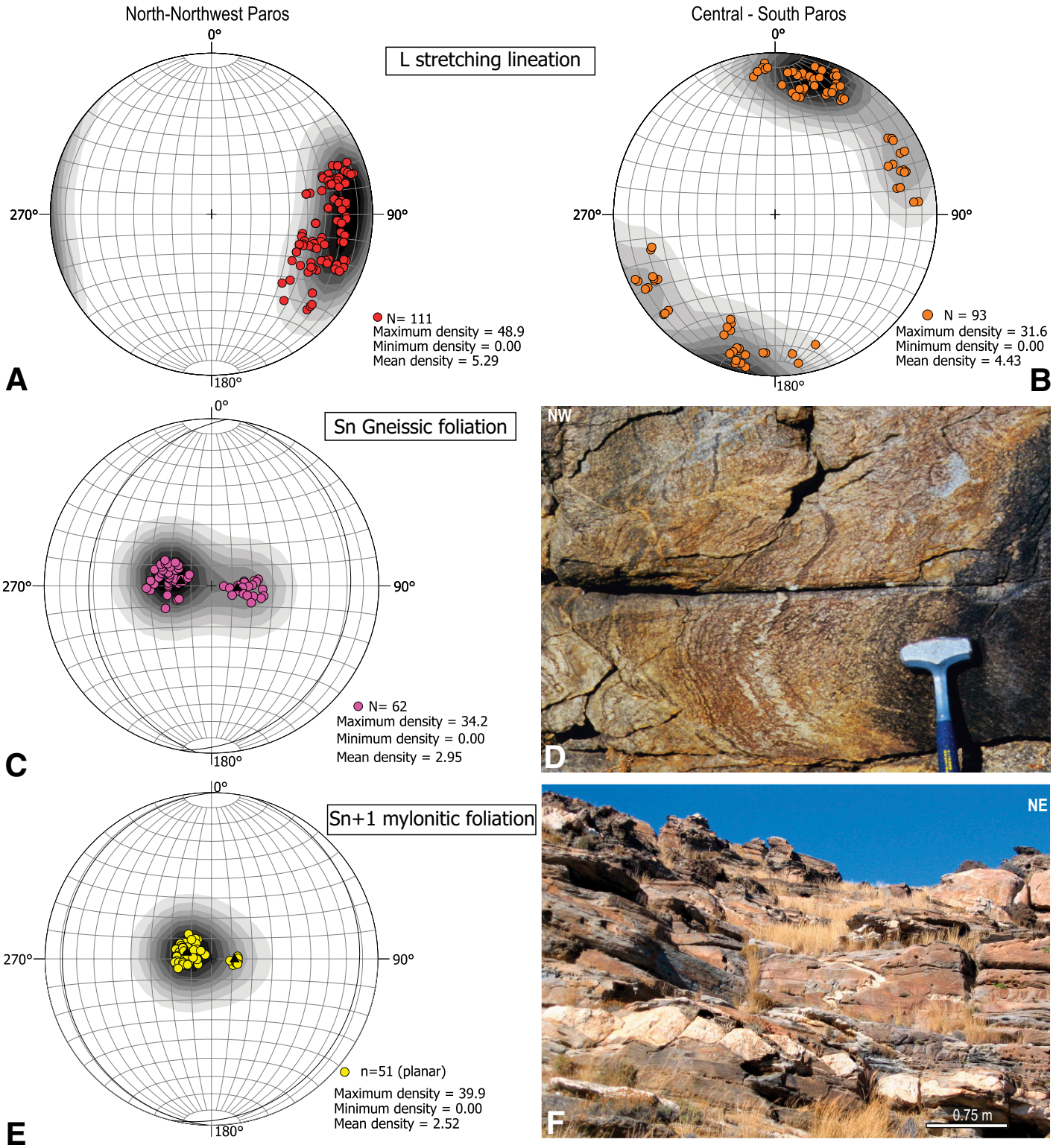

Figure 5. (A–B) Stereoplots (equal-area lower-hemisphere projection) showing the orientation of the stretching lineation at the north-northwestern (A) and the central-southern part of Paros Island (B), where E-ESE and N-NW trends prevail, respectively. The ENE to NE measurements in both areas are located mostly along the eastern flank of the Paroikia-Naoussa valley, and they are related to the influence of the Elitas shear zone. (C) Stereoplot (equal-area lower-hemisphere projection) of poles to gneissic foliation in the pre-Alpine orthogneiss. The distribution of measurements reveals a gentle NNE-SSW antiform. (D) Close-up view of the gneissic foliation in the orthogneiss folded with NE-SW recumbent folds. (E) Stereoplot (equal-area lower-hemisphere projection) of poles to mylonitic foliation. (F) Domino-type boudinage and asymmetric folding in aplitic intrusions within the orthogneiss at the northernmost part of Paros Island. Sense of shear in this area is top-to-the-NE. (*Continued on following page.*)

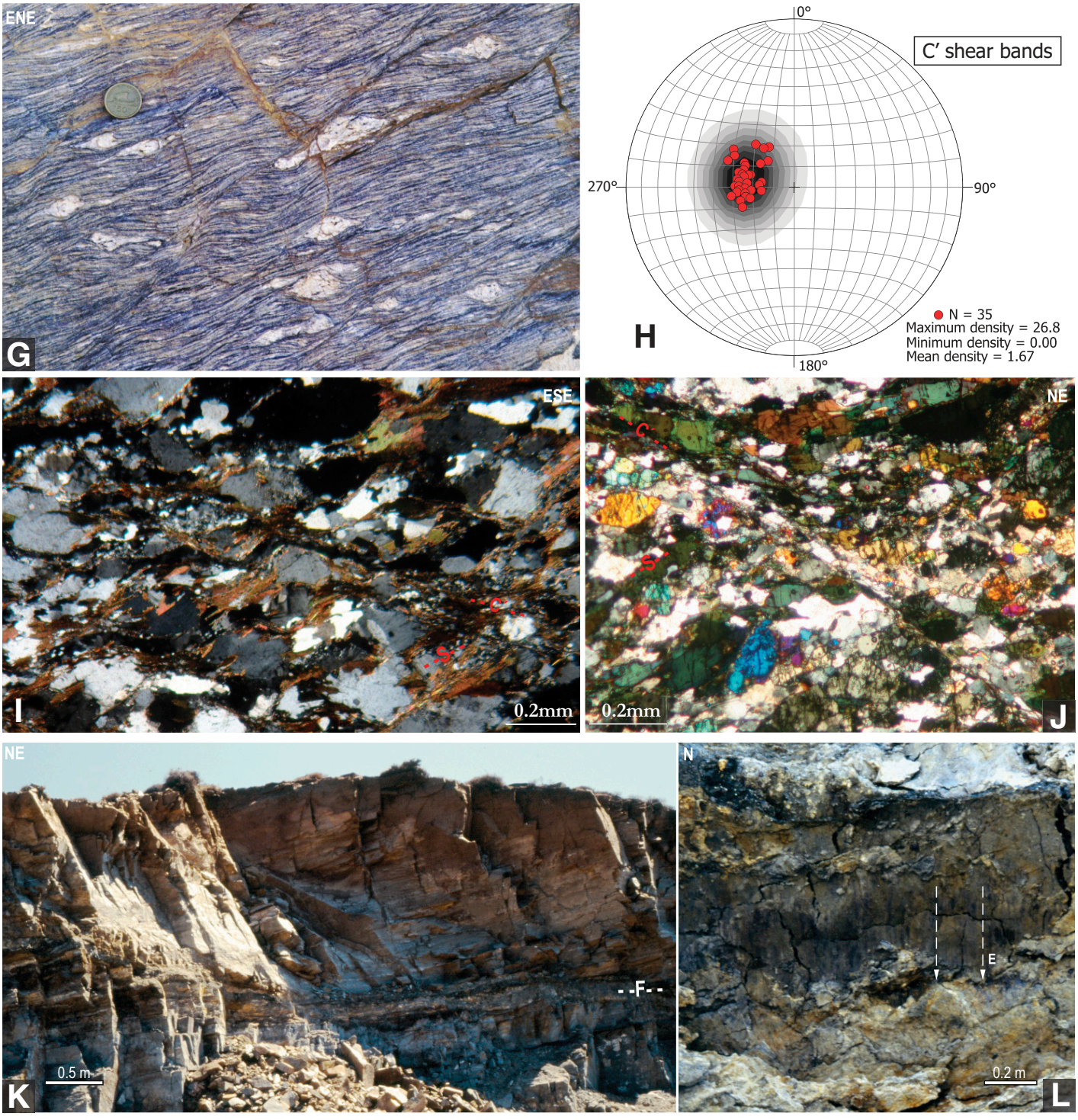

Figure 5 (*continued*). (G) C′ shear bands cutting through the mylonitic foliation and tension gashes of the orthogneiss and forming a S-C′ fabric. Sense of shear is top-to-the-ENE. (H) Stereoplot (equal area, lower hemisphere) of poles to C′ surfaces in north Paros. (I) Photograph in the microscopic scale showing C′ shear bands deforming the Sn+1 mylonitic foliation in the orthogneiss. The Sn+1 foliation is formed by coarse-grained quartz aggregates, boudinaged feldspars, and micas, and the C′ plane is formed by recrystallized quartz and/or micas. Sense of shear is top-to-the-NE. (J) Photograph in the microscopic scale showing C′ shear bands in the amphibolitic rocks of Marathi Unit, deforming the amphibolite-facies Sn foliation and forming an S-C′ fabric. Sense of shear is top-to-the-NE. (K) Late-stage low-angle cataclastic fault zone (F) within the orthogneisses structurally a few meters below the contact with the overlying Marathi marbles. (L) Detail of the previous photo showing a clay gouge formed in a secondary steeper fault in that zone bearing E-dipping striations (white arrows).

deformation becomes localized toward the contact with the overlying units. The footwall is dominated by the structurally deeper pre-Alpine basement orthogneisses, whereas the hanging wall is dominated by the structurally higher Marathi Unit, but both units are present in both hanging wall and footwall.

As mentioned previously, the older foliation that is identified in the footwall orthogneisses is a gneissic foliation formed by the alternation of layers rich in quartz and feldspars with layers that mostly include biotite and/or white micas. In the northern part of the island, the gneissic foliation generally dips east, but closer to the NW coast, it is bent to the west, thus forming a broad NNE-SSW antiform (Fig. 5C). It should be noted that this antiform is not parallel to the approximately E-W local trend of the stretching lineation, as usually occurs with extension-parallel folds. This foliation is probably related to the amphibolite-facies metamorphism that is much better identified in the overlying Marathi Unit amphibolites. The mineral composition of the orthogneiss does not reveal much evidence of that stage, but in the microscopic scale, recrystallization of feldspars can be observed. Locally, the gneissic foliation is folded with tight to isoclinal folds, which are probably contemporaneous with the refolding folds in the overlying Marathi Unit (Fig. 5D; 37°4′0.27″N, 25°9′23.31″E).

At the northern part of the island, a strain gradient is observed at the structurally higher levels of the orthogneiss. An E-dipping mylonitic to ultramylonitic foliation is developed below the contact with the marbles of Marathi Unit and above the intrusion level of the granitic rocks (Figs. 4H and 5E). The mylonitization of the orthogneisses has a semiductile character, where alkali-feldspars and plagioclase exhibit brittle deformation (brittle fractures that evolve to domino-type or shear-band boudinage), whereas biotite, white micas, and quartz have recrystallized to form the mylonitic foliation. In many cases, structurally below the level of mylonitization, the gneissic foliation is folded asymmetrically, and a new axial planar flat-lying foliation is formed subparallel to the mylonitic foliation. This event was accompanied by the development of stretching lineations formed by elongated quartz aggregates of mica-fish and trains of feldspar grains that now trend approximately E-W to NE-SW. The E-W trends are observed at the northern part of the island. The NE-SW trend is observed along a narrow NE-SW–trending zone, which is located along the eastern flank of the Paroikia-Naoussa valley (Fig. 3). In this area, a mylonitic foliation can be also observed in the overlying rocks of the Marathi Unit. It is noteworthy that the change of the stretching lineation trend toward the NE observed in the pre-Alpine basement units is reflected in a similar change in direction of the mode I extensional cracks within the Marathi Unit. The mylonitic deformation has variably deformed the aplitic and pegmatitic veins that have intruded the orthogneiss, forming shear-band and domino-type boudinage as well as asymmetric folds (Figs. 4H and 5F; 37°8′49.28″N, 25°13′30.18″E).

Throughout the northern part, the mylonitic foliation is cut by C′-type shear bands (Fig. 5H; 37°8′9.17″N, 25°12′55.10″E) that dip generally toward the east and locally toward northeast (Fig. 5H), which could be an indication that they are affected by the gentle NNE-SSW, large-scale folding. In general, the density of C′ planes increases toward the contact with the Marathi Unit. Even in the less-deformed parts of the basement, the C′ planes are visible under the microscope, forming an S-C′ fabric with the minerals that constitute the gneissic foliation (Fig. 5I). In a few cases, they are accompanied by an E-plunging lineation formed by strained minerals that are stretched or crenulated by extension-parallel folds. A similar S-C fabric can be observed within the overlying amphibolitic rocks of Marathi Unit, especially under the microscope (Fig. 5J).

A younger set of high-angle fractures or minor faults that crosscut all the previous structures marks the passage to brittle conditions (Fig. 5G). Brittle deformation is mostly observed near, but not restricted to, the contact between the orthogneiss and the Marathi Unit along the shear zone (Fig. 4G). Along this contact, a thick zone of fault breccia, reaching up to 5 m, is formed by angular clasts from both lithologies, thus obliterating the ductile structures (exactly north of Paroikia; 37°5′11.78″N, 25°10′22.09″E). These fault breccias are usually associated with low-angle (Fig. 5K; 37°7′27.74″N, 25°11′10.89″E) or high-angle cataclastic fault zones that produced cohesive to incohesive cataclasites. In few places, steeper cataclastic zones with approximately E-plunging slickenlines are observed (Fig. 5I; 37°7′27.74″N, 25°11′10.89″E).

Numerous structures (e.g., boudinaged veins, σ-clasts, S-C′ fabric, domino-type and shear-band boudinage of feldspar grains, and striations on fault surfaces) indicate a top-to-the-E sense of shear for the northern part of the island (Figs. 4G, 5F, 5G, 5I, 5J, and 5L), contrary to the central-south parts, where the sense of shear is top-to-the N (Figs. 4A–4B).

Based on these observations, we infer that this area is affected by a NNE-SSW semiductile to brittle, top-to-the-E shear zone, here identified as the Elitas shear zone, which represents an extensional shear zone, or detachment, that cuts through the older, higher-temperature gneissic foliation of the pre-Alpine basement and Marathi Units. The northern part of the island constitutes the footwall, and the central and eastern parts occupy the hanging wall to that detachment. The continuation of the Elitas shear zone south of Paroikia is obscured by poor exposure, but we infer its continuation from the gradual change of stretching lineation orientations that continues all the way to the southwest.

SAMPLING AND METHODS

To analyze whether the change in stretching lineations on Paros Island resulted from vertical-axis rotations after formation of these lineations, we collected a total of 160 oriented paleomagnetic cores from 16 sites in granitoids, homogeneously distributed across the island (Fig. 3; Table 1). Samples were collected from intrusions represented by Middle–Late Miocene S-granites, and aplitic and quartzitic veins. Granites within the pre-Alpine basement were sampled at 11 sites; four sites were sampled within aplitic (three sites) and quartzitic (one site) veins, which intruded simultaneously with or slightly after the granites; one site was sampled from an Upper Miocene rhyolitic dike.

Cores were cut into standard paleomagnetic samples and then analyzed in the Fort Hoofddijk paleomagnetic laboratory (Utrecht University). About 60% of the specimens were demagnetized using thermal treatment, while the remaining samples were subjected to alternating field (AF) demagnetization. Thermal demagnetizations were performed by applying 30 °C step increments from room temperature up to 580 °C (or earlier complete demagnetization of the sample). AF demagnetizations were carried out by applying 5 mT step increments from 5 mT up to 100 mT. Magnetic remanence was measured after each demagnetization step using a 2G Enterprises DC SQUID cryogenic magnetometer (noise level 3×10^{-12} Am^2). Demagnetization data were plotted on orthogonal diagrams (Zijderveld, 1967), and the magnetization components were isolated via principal component analysis (Kirschvink, 1980) using the online software package for paleomagnetic analysis on www.paleomagnetism.org (Koymans et al., 2016). All demagnetization diagrams and statistical analyses are included in the GSA Data Repository[1] as files that can be uploaded and viewed on this Web site. Only computed directions showing maximum angle of deviation

[1]GSA Data Repository Item 2016359, demagnetization diagrams and statistical analyses in paleomagnetism.org format that can be uploaded and viewed in the pmag.org tool, is available at www.geosociety.org/pubs/ft2016.htm, or on request from editing@geosociety.org.

TABLE 1. PALEOMAGNETIC RESULTS FROM PAROS ISLAND

Site	Lithology	Latitude (°N)	Longitude (°E)	*N*	N_{45}	*D* (°)	Δ*D* (°)	*I* (°)	Δ*I*	*k*	α_{95} (°)	*K*	A_{95} (°)	A_{95min} (°)	A_{95max} (°)
P1	S-granite	37.11699	25.18168	13	13	112.7	10.1	49.7	9.8	35.2	7.1	23.6	8.7	4.3	16.3
P2	S-granite	37.11835	25.18858	16	15	103.4	14.4	59.3	9.8	27.4	7.4	13.1	11.0	4.1	14.9
P3	S-granite	37.12557	25.20940	13	13	072.0	4.2	50.5	3.9	162.9	3.3	136.8	3.6	4.3	16.3
P4*	S-granite	37.05601	25.17196	14	–	–	–	–	–	–	–	–	–	–	–
P5	Aplitic vein	37.07887	25.21037	15	13	020.2	8.8	25.7	14.8	17.2	10.3	24.2	8.6	4.3	16.3
P6	S-granite	37.03913	25.19551	14	12	349.0	7.0	27.3	11.3	35.8	7.4	42.5	6.7	4.4	17.1
P7*	Aplitic vein	37.01620	25.23998	7	5	341.1	26.3	22.0	46.1	9.3	26.5	9.8	25.8	6.3	29.7
P8	Aplitic vein	37.01716	25.23922	8	6	350.4	11.2	19.9	20.2	16.7	16.9	37.6	11.1	5.9	26.5
P9	S-granite	37.03738	25.19604	12	12	329.5	12.8	33.0	18.9	13.1	12.5	13.7	12.2	4.4	17.1
P10	S-granite	37.12326	25.20688	12	12	090.9	9.1	49.7	8.8	36.7	7.3	31.6	7.8	4.4	17.1
P11	S-granite	37.12692	25.20966	15	12	075.1	5.5	52.8	4.9	118.9	4.0	88.7	4.6	4.4	17.1
P12	Quartz vein	37.00694	25.24219	17	13	349.0	10.4	34.3	15.0	12.9	12.0	18.8	9.8	4.3	16.3
P13*	Rhyolite dike	37.13611	25.20968	17	–	–	–	–	–	–	–	–	–	–	–
P14	S-granite	37.12909	25.21331	10	9	056.7	12.2	57.1	9.0	40.7	8.2	29.7	9.6	5.0	20.5
P15	S-granite	37.11962	25.19220	9	7	108.7	17.1	40.8	21.3	16.3	15.4	15.8	15.7	5.5	24.1
P16	S-granite	37.11080	25.17237	15	13	112.6	9.2	36.1	12.8	22.1	9.0	23.8	8.7	4.3	16.3

Note: *N*—number of specimens analyzed; N_{45}—number of specimens used for the computation of the mean values after filtering by a 45° cutoff; *D*, *I*—in situ (geographic) mean declination and inclination; d*D*, d*I*—error margin on declination and inclination; *k* (*K*) —precision parameter of the characteristic direction (virtual geomagnetic pole) distribution; α_{95} (A_{95})—semi-angle of the 95% confidence cone around the mean direction (mean virtual geomagnetic pole); A_{95min}, A_{95max}—minimum and maximum A_{95} value expected for a paleosecular variation-induced scatter according to Deenen et al. (2011).
*Discarded site (see text for explanation).

smaller than 15° were used for the calculation of site-mean values.

Site-mean directions were evaluated using a Fisher statistic (Fisher, 1953) on virtual geomagnetic poles (VGPs) corresponding to the characteristic remanent magnetizations (ChRMs) after applying a fixed 45° cutoff (Johnson et al., 2008). Applying the Fisher statistic on VGPs rather than paleomagnetic directions for the computation of the site-mean values is preferred because it allows more realistic error estimates on the declination (*D*) and inclination (*I*) values (Deenen et al., 2011). Following criteria proposed by Deenen et al. (2011), we compared the VGP scatter (indicated by the A_{95} value) calculated at each site with the scatter of a similar data set produced by paleosecular variation (PSV; indicated by the A_{95min} and A_{95max} values). A PSV not adequately represented within the data set (i.e., $A_{95} < A_{95min}$) indicates insufficient time averaging, or remagnetization. Conversely, overrepresentation of PSV (i.e., $A_{95} > A_{95max}$) may point out additional processes responsible for the scatter of the paleomagnetic directions (e.g., high internal deformation or lightning strike influence).

The nature of the main magnetic carriers in the studied rocks was determined through the analysis of the Curie temperatures obtained from the thermal demagnetizations and Curie balance measurements. Horizontal translation Curie balance experiments (Mullender et al., 1993) were carried out on one representative sample per site. Specimens were crushed into powder and subsequently subjected to stepwise heating-cooling cycles from room temperature up to 700 °C.

Together with paleomagnetic analyses, we have carried out analyses of the AMS to test the extent to which the magnetic minerals in the sampled granitoids may have been affected by shearing, producing a mineral preferred orientation that may have influenced the natural remanent magnetization. AMS analyses of all samples were performed using an AGICO MFK1 Kappabridge, and the AMS tensors were evaluated using a Jelínek's statistics (Jelínek, 1977; Jelínek and Kropácek, 1978).

AMS is a petrofabric tool commonly used to determine the preferred orientation of magnetically dominant minerals (Jelínek, 1977; Jelínek and Kropácek, 1978; Hrouda, 1982; 1993; Borradaile, 1991, 1988). AMS is geometrically described by an ellipsoid with minimum (k_{min}), intermediate (k_{int}), and maximum (k_{max}) axes of susceptibility (e.g., Hrouda, 1982). During deformation, the three susceptibility axes realign according to the local strain field, yielding an AMS ellipsoid that is comparable both in shape and orientation to the strain ellipsoid (e.g., Parés et al., 1999). Similar to the strain ellipsoid, it is possible to identify an oblate ($k_{max} \approx k_{int} >> k_{min}$), triaxial ($k_{max} > k_{int} > k_{min}$), or prolate AMS ellipsoid ($k_{max} >> k_{int} \approx k_{min}$). In particular, the k_{max} axis, which defines the magnetic lineation (L), commonly develops parallel to the maximum stretching axis (ε_1), and hence parallel to the mineral stretching lineation (Sagnotti et al., 1994; Mattei et al., 1997, 1999; Cifelli et al., 2004, 2005; Maffione et al., 2012, 2015). A magnetic foliation (F), identified by the clustering of the k_{min} axes, will instead form parallel to the mineral foliation or to the schistosity planes in highly strained rocks.

RESULTS

Rock Magnetism

Remanence decay curves obtained from both thermal and AF demagnetizations and the Curie balance experiments show the occurrence of different ferromagnetic minerals characterized by variable Curie temperatures and coercivity. Seven sites within granite and aplitic veins (P3, P4, P5, P7, P8, P15, and P16) show Curie temperatures between 150 °C and 580 °C and low coercivity (80%–100% of the remanence was demagnetized at 100 mT), suggesting the occurrence of low- to high-Ti titanomagnetite as the main carrier of magnetization (Fig. 6). Another seven sites within granite and quartzitic veins (P1, P2, P6, P10, P11, P12, and P14) show Curie temperatures between 200 °C and 580 °C and medium to high coercivity (20%–50% of the remanence was demagnetized at 100 mT), interpreted as indicating the presence of a mixture of titanomagnetite and iron sulfides (likely pyrrhotite; Fig. 6). Two remaining sites in granite (P9) and rhyolitic dikes (P13) are characterized by higher Curie temperatures in the range of 500–650 °C and 200–680 °C, and medium to low coercivity (40%–100% of the remanence was demagnetized at 100 mT), respectively. This suggested the occurrence of a mixture between low- to high-Ti titanomagnetite and possibly secondary maghemite resulting from low-temperature oxidation processes (Fig. 6). Minor occurrence of maghemite may also be inferred at sites P4 and P14, where very high Curie temperatures (680 °C) were observed

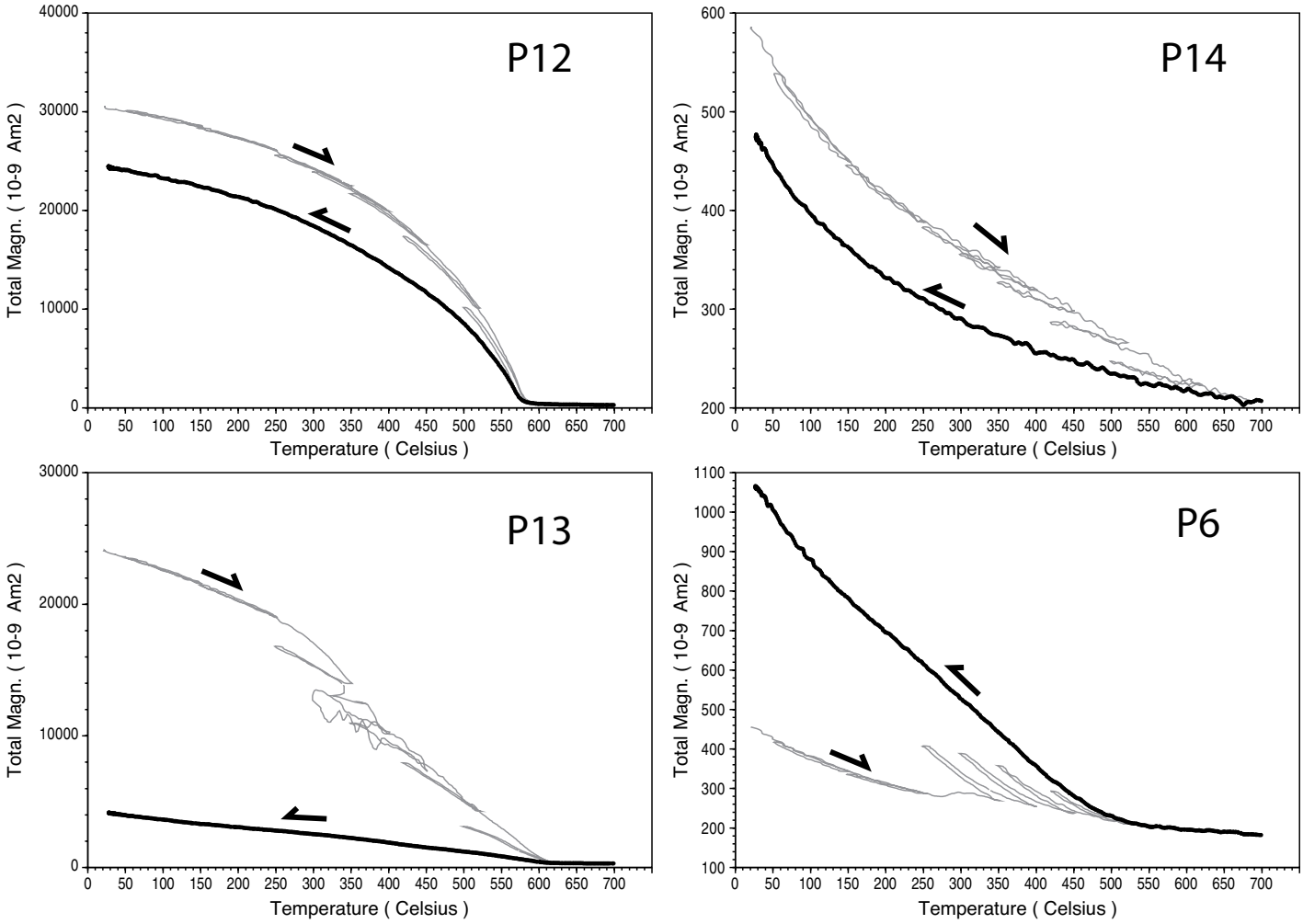

Figure 6. Results for the Curie balance experiments from representative samples from granites, quartzitic veins, and rhyolitic dikes. Heating (stepwise) and cooling curves are represented by gray and black lines, respectively.

from the Curie balance experiments, likely due to the formation of hematite upon maghemite breakdown occurred during heating.

Paleomagnetism

Natural remanent magnetization (NRM) intensities of the studied samples identify two main groups: granites and aplitic veins characterized by very weak magnetizations in the range of 0.1–6 mA/m, and quartzitic veins and rhyolitic dikes showing higher intensities from 20 mA/m to 3.5 A/m. Thermal demagnetization treatment was found to be more effective than AF in removing the NRM of the samples due to the common occurrence of high-coercivity mineral phases. However, even when AF demagnetization was not complete, a high-stability component (interpreted as the ChRM) decaying toward the origin of Zijderveld diagram could be identified. ChRM components were isolated from all of the studied samples at high temperatures of ~600 °C (using demagnetization steps from 250 °C to 600 °C) and high AF of 100 mT (using steps 20 mT and 100 mT), except sites P12 (quartzitic veins) and P13 (rhyolitic dikes), where the ChRMs were isolated at temperatures higher than 650 °C (Fig. 7).

Variable numbers of specimens per site (7–15) were used to compute the mean directions shown in Table 1. Statistically well-defined site-mean values were computed at 13 out of 16 sites. Directions isolated at three sites (P4 and P7 in granite and P13 in the Upper Miocene rhyolitic dike) were highly scattered and not statistically meaningful. The computed mean values from 13 sites satisfied standard quality criteria for paleomagnetic analyses ($A_{95} < A_{95max}$; sensu Deenen et al., 2011). The VGP scatter at site P3 (granite) was smaller than expected from PSV (i.e., $A_{95} = 3.6 < A_{95min} = 4.4$; sensu Deenen et al., 2011), which we interpret as the result of an incomplete time averaging of PSV. Because the direction of P3 was very similar to those of the surrounding sites, we include it in our further analysis. Based on the VGP distributions of each site and the calculated in situ directions, which are substantially different from the present-day geocentric axial dipole field direction in Paros (D/I = 000°/56°), we interpret the magnetization as primary, acquired upon cooling of the sampled granitoid bodies below the Curie temperature. All sites recorded a normal polarity, which was pertinent for ~60% of the Middle Miocene (Gradstein et al., 2012).

Overall, the 13 calculated in situ-mean directions form two clusters (Fig. 8). Eight sites from northern Paros (P1, P2, P3, P10, P11, P14, P15, P16) show mainly E-directed paleomagnetic directions, which share a common mean direction with D = 91.7° ± 4.6° and I = 50.9° ± 4.3° (N/N_{45} = 105/90; K = 15.8; A_{95} = 3.9°; $A_{95min/max}$ = 2.0°/4.8°). Five sites from the central-southern

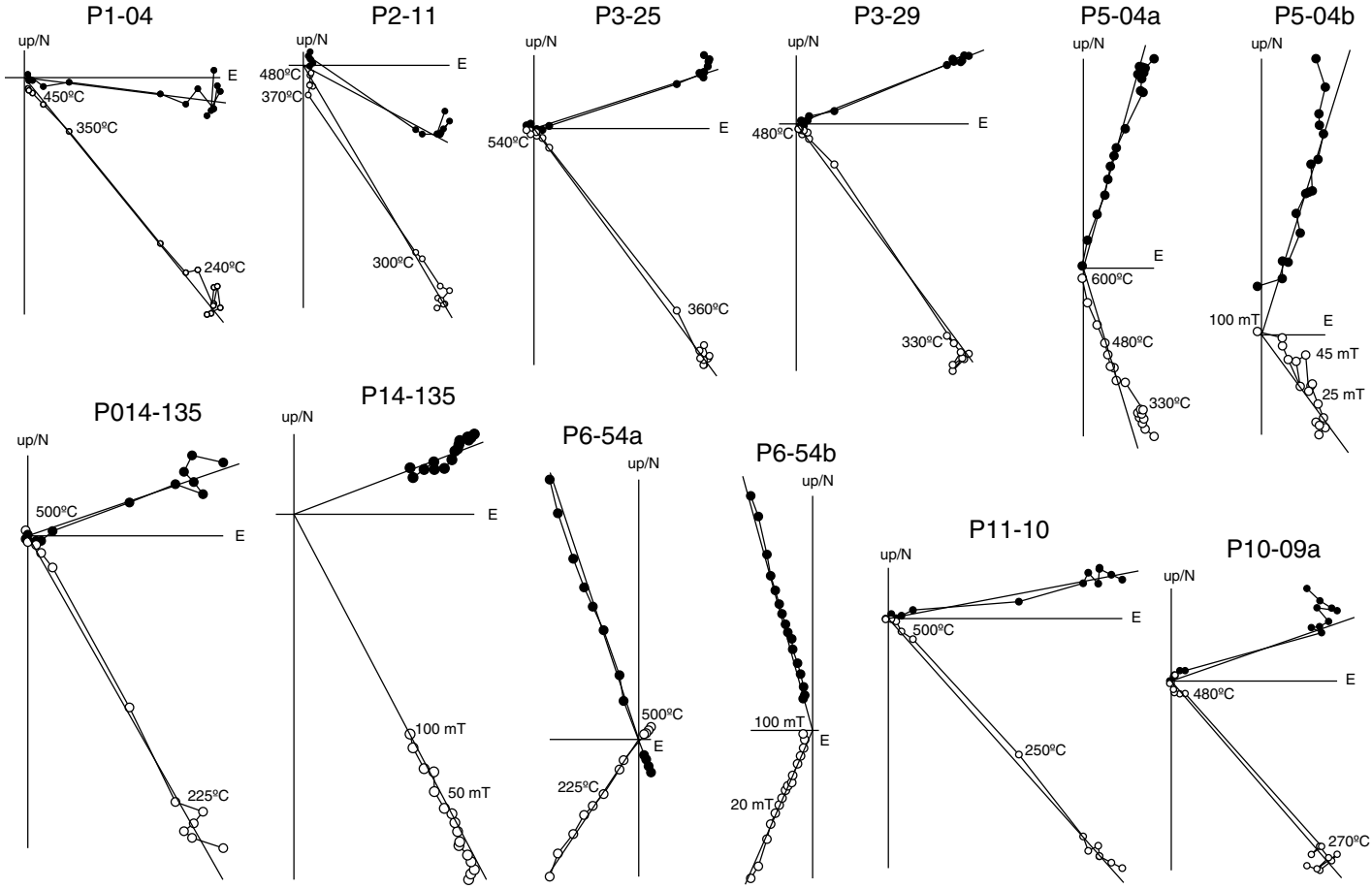

Figure 7. Zijderveld diagrams (Zijderveld, 1967) of representative samples demagnetized using both thermal (TH) and alternating field (AF) treatment shown with in situ coordinates. Solid and open dots represent projections on the horizontal and vertical planes, respectively. Demagnetization step values are in °C or in mT. The isolated characteristic remanent magnetization (ChRM) component is shown in each diagram.

part of Paros (P5, P6, P8, P9, P12) show mainly N-directed paleomagnetic directions characterized by a common direction with $D = 355.1° \pm 4.6°$ and $I = 29.1° \pm 7.3°$ ($N/N_{45} = 64/49$; $K = 22.1$; $A_{95} = 4.4°$; $A_{95min/max} = 2.5°/7.1°$; Fig. 8). Both of these mean directions from northern and southern Paros satisfy Deenen's criteria (Deenen et al., 2011) and were used for further tectonic interpretations. In addition, we performed the orocline test of Pastor-Galán et al. (2016), also available on www.paleomagnetism.org, to test the correlation between the direction of structural features (in this specific case, the magnetic lineations) and the vertical-axis rotations. A positive orocline test is obtained when the calculated change in direction of a structure across a given area is reflected by an equivalent variation of the paleomagnetic declination.

The orocline test performed using the stretching lineations from the basement and the paleomagnetic declinations from the granitoids that intrude the basement in Paros resulted in a positive orocline test (Fig. 9). This demonstrates that at the time of intrusion of the granitoids, the stretching lineations from both the north and south domains of Paros were parallel and N-S–trending features; this parallel system of stretching lineations was subsequently disrupted due to relative rotations of crustal domains across Paros.

AMS

Results from the AMS analysis are shown in Figure 10 and Table 2. The corrected degree of anisotropy (P′) for all sites was between 1.011 and 1.171, indicating that the internal fabric of the studied rocks has been affected by a variable degree of anisotropy. This is also supported by the relatively high lineation (L) and foliation (F) values (Table 2). Despite this, the directions of the maximum, intermediate, and minimum susceptibility axes at the site level appear highly scattered at all sites, except P7, P8, and P12 (aplitic and quartzitic veins), where a weak triaxial AMS ellipsoid with a roughly N-S–oriented magnetic lineation can be observed.

Even when all AMS results are combined and shown separately for the northern and southern sector of Paros (characterized by approximately E- and approximately N-directed paleomagnetic directions, respectively), the directions of the three susceptibility axes appear scattered, and no systematic mean magnetic lineation for both areas is apparent. From this, we can conclude that the magnetic mineral distribution within the granitoid rocks is essentially isotropic, and that the paleomagnetic directions for the northern and central-southern domain of Paros are unrelated to the magnetic fabrics of the sampled rocks. Even if highly scattered, most of the magnetic lineations that can be measured have a direction that is substantially different and that varies widely from the mean paleomagnetic direction in each of the two domains of Paros.

DISCUSSION

Vertical-Axis Rotations on Paros Island

Paleomagnetic and rock magnetic results from Miocene intrusive rocks (granitoids, veins, and dikes) of Paros Island show a stable and

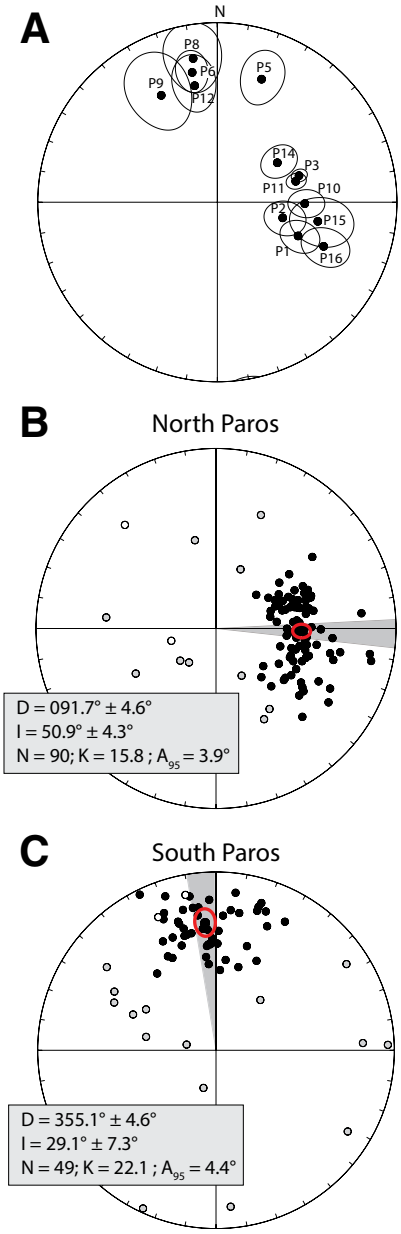

Figure 8. Lower-hemisphere equal-area stereographic projections showing the in situ directions of the isolated characteristic remanent magnetization (ChRM) component from the studied sites. (A) Site-mean directions and associated ellipses of confidence. (B, C) Distributions of the single ChRM values from (B) the eight sites in northern Paros showing mainly E-directed site-mean directions, and (C) the five sites from southern Paros showing mainly N-directed site-mean directions. Mean paleomagnetic directions and statistical parameters are shown for both northern and southern Paros. Red ellipse is the cone of the 95% confidence around the mean value. Shaded gray areas indicate the uncertainty on the calculated mean declination. D—Declination; I—Inclination; N—number of directions used for average; K—Fisher (1953) precision parameter; A_{95}—95% confidence limit on the virtual geomagnetic poles.

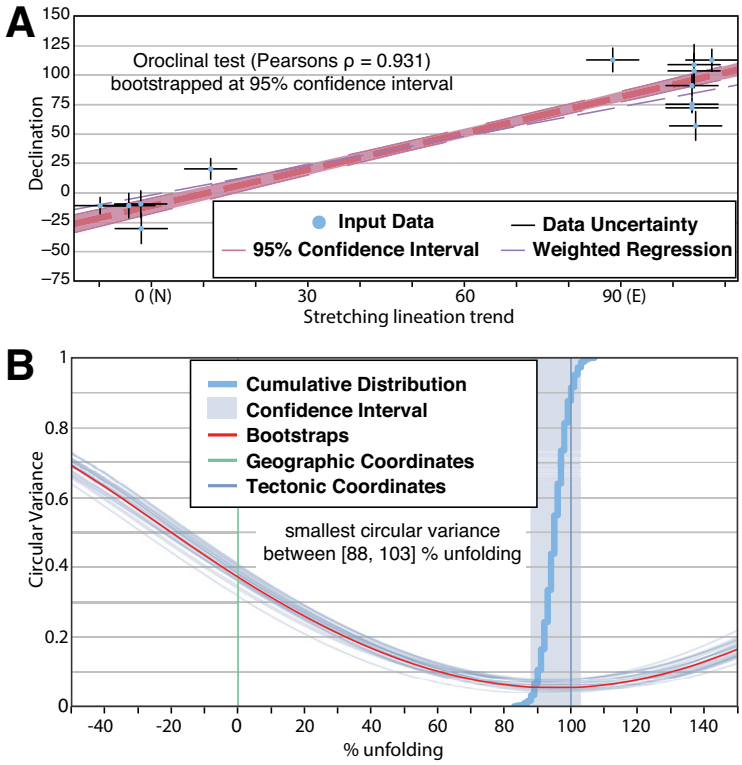

Figure 9. (A) Orocline test of Pastor-Galán et al. (2016) showing the sampled declinations and strikes (blue dots) with measurement uncertainties (black bars). The red line shows the total least squares regression for the data. The surrounding shaded red area illustrates the confidence interval for 1000 bootstrapped regressions. (B) Oroclinal fold test showing the circular variance as a function of unfolding. A smaller circular variance indicates a tighter clustering of the data. The bold red line and nearby blue lines represent the actual data and the first 25 bootstraps, respectively.

well-defined magnetic remanence at 13 sites (Fig. 8; Table 1). These directions differ from the present-day field, contain scatters that well represent PSV, and are unrelated to mineral preferred orientations in the sampled granitoids. We interpret these directions as "primary," acquired during cooling of the sampled granitoid bodies below the Curie temperature (up to 580 °C, i.e., during cooling through greenschist-facies conditions). The intrusion age of the granitoids is ca. 16 Ma (Bargnesi et al., 2013), and zircon fission-track ages indicate that the metamorphic rocks of Paros cooled below ~200 °C by 13–11 Ma (Brichau et al., 2006). From this, we estimate that the magnetization was recorded sometime between 16 and 13 Ma.

Paleomagnetic directions from these 13 sites form two clusters with an organized spatial pattern: Five sites from the central-southern sector of Paros show a mainly N-S–directed paleomagnetic direction (D = 355.1° ± 4.6° and I = 29.1° ± 7.3°), while eight sites within the northern area of Paros display mainly eastward directions (D = 091.7° ± 4.6° and I = 50.9° ± 4.3°).

These directions represent in situ magnetizations, i.e., not corrected for tectonic tilt, which we cannot constrain given the absence of paleohorizontal data (e.g., bedding). Their high consistency within the northern and central-southern domain of Paros, however, excludes the possibility that significant internal deformation (i.e., between sites of each cluster) occurred after remanence acquisition. Furthermore, the mean paleomagnetic inclination for the northern domain of Paros coincides with the expected inclination at the sampling location during the Miocene for stable Europe (54° ± 2°; Torsvik et al., 2012), suggesting that no major net tilt has occurred during the exhumation of these rocks. The shallower mean inclination calculated for the central-southern domain of Paros suggests an overall southward tilt of these rocks of perhaps 20°. This may be supported by the southward decrease of the metamorphic grade within the Marathi Unit proposed by Robert (1982). Whereas such southward tilt would affect the inclination, it would have little influence on the still northward-directed declination.

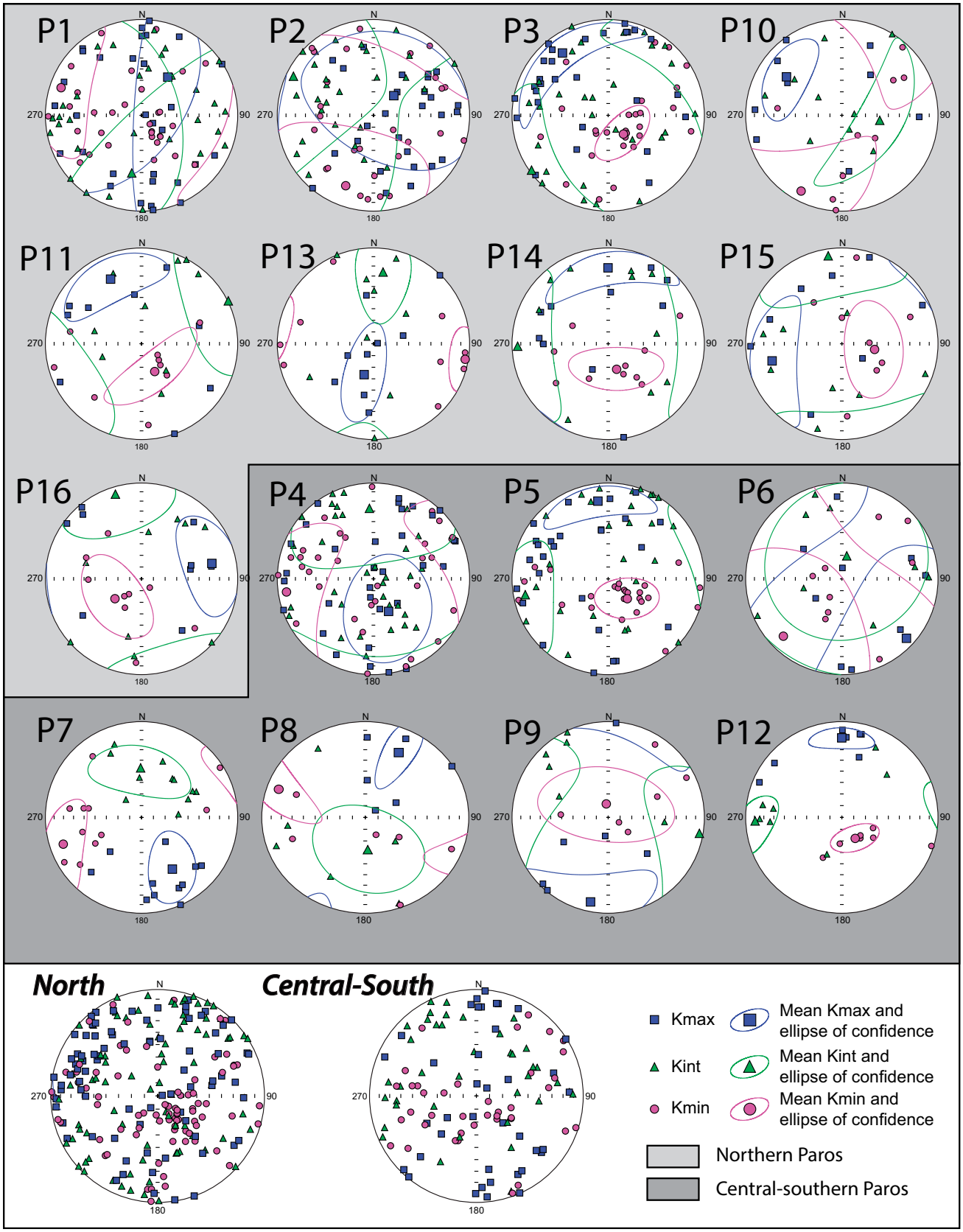

Figure 10. Lower-hemisphere equal-area stereographic projections of the (in situ coordinates) principal axes (k_{max}, k_{int}, and k_{min}) of the anisotropy of magnetic susceptibility (AMS) ellipsoid from all sampled sites. Mean values of the three susceptibility axes (larger symbols) and relative 95% confidence ellipses are shown for each diagram. AMS plots from northern and southern Paros are identified by a different background color.

TABLE 2. ANISOTROPY OF MAGNETIC SUSCEPTIBILITY (AMS) RESULTS FROM PAROS ISLAND

Site	Lithology	*N*	*k*m	L	F	P'	T	*D* (°)	*I* (°)	*e*12 (°)
Northern Paros										
P1	S-granite	31	819	1.008	1.042	1.059	0.718	034.4	50.0	87.6
P2	S-granite	27	958	1.004	1.018	1.024	0.608	045.9	65.9	81.9
P3	S-granite	28	900	1.015	1.047	1.065	0.512	323.8	20.5	60.4
P10	S-granite	9	67.9	1.029	1.011	1.042	-0.431	304.9	30.5	33.9
P11	S-granite	9	87.9	1.030	1.034	1.065	0.059	334.5	26.2	42.9
P13	Rhyolitic dike	9	10900	1.007	1.024	1.032	0.537	196.7	62.5	45.4
P14	S-granite	10	83.1	1.022	1.051	1.076	0.385	359.9	21.9	51.7
P15	S-granite	8	76.6	1.030	1.045	1.077	0.195	256.1	26.2	52.2
P16	S-granite	9	73.5	1.032	1.043	1.077	0.146	077.6	26.1	38.8
Central Southern Paros										
P4	S-granite	32	850	1.026	1.029	1.056	0.046	155.1	59.3	48.5
P5	Aplitic vein	26	1140	1.023	1.054	1.081	0.401	352.5	19.3	41.6
P6	S-granite	9	176	1.005	1.006	1.011	0.117	132.8	9.4	71.0
P7	Aplitic vein	11	13.4	1.036	1.021	1.059	–0.261	149.3	37.3	33.4
P8	Aplitic vein	6	13.1	1.045	1.031	1.078	–0.175	025.5	25.9	37.4
P9	S-granite	6	147	1.022	1.015	1.038	–0.184	191.8	10.9	50.5
P12	Quartzitic vein	7	2040	1.096	1.067	1.171	–0.172	359.9	18.1	22.9

Note: *N*—number of studied samples at a site; k_m—site-mean susceptibility in 10^{-6} SI. Magnetic lineation (L), magnetic foliation (F), corrected anisotropy degree (P′), and shape factor (T) are given according to Jelinek (1981). *D* and *I* are the in situ site-mean declination and inclination, respectively, of the maximum susceptibility axis (k_{max}); e_{12}—semi-angle of the 95% confidence ellipse around the declination of the k_{max}.

Alternatively, the rotation difference could be an artifact of a horizontal-axis rotation parallel to the Elitas shear zone, i.e., ~50°E. The rotation difference could be explained if a horizontal-axis rotation difference of ~85° had occurred. Since the rotations postdate granitoid intrusion, which in turn postdates the regional foliation, the foliation on the NW and SE side of the island should then be near-orthogonal to each other, which they clearly are not. From this, we infer that we may use the declinations obtained from these granitoids as evidence for vertical-axis rotations, and so we use these for further analysis of the tectonic history of Paros.

The sampled granitoids cut the regional foliation that formed at high metamorphic grades, and the magnetic susceptibility (AMS) from all sampled units further demonstrates that the granitoids were not significantly affected by this distributed ductile deformation. The intrusion of the granitoids, therefore, postdates the ductile fabrics defined by pervasive mineral foliation and widespread stretching lineations, which were dated to range from 23 and 16 Ma, in the few million years prior to granitoid intrusion (Gautier et al., 1993; Avigad et al., 2001; Bargnesi et al., 2013; Jolivet et al., 2015). This suggests that the granitoids intruded after cooling and exhumation of the Cycladic Blueschist Unit and pre-Alpine basement units of Paros to greenschist-facies conditions, at which time further exhumation was accommodated along discrete detachments.

It is then interesting to note that the measured declinations in the granitoids are subparallel to the stretching lineations in the metamorphic host rocks into which the granitoids intruded. From this, we may draw the following conclusions. First, at the time the granitoids intruded, the stretching lineations of both the northern and southern domains were parallel and trending approximately N-S to NNE-SSW. This shows that during the first stages of exhumation from amphibolite- to greenschist-facies metamorphic conditions (ca. 23–16 Ma), there were likely no vertical-axis rotations on the island of Paros. Second, after intrusion and during final exhumation, the northern part of Paros Island underwent a major clockwise rotation relative to the southern domain. When compared to the expected Middle Miocene declination of Eurasia of (4 ± 2°; Torsvik et al., 2012), the northern domain rotated ~90° clockwise, and the southern domain rotated ~10° counterclockwise.

Structural Accommodation of Vertical-Axis Rotations on Paros Island

Our paleomagnetic analysis demonstrates that the transition between easterly and northerly directed stretching lineations, regionally identified as the Mid-Cycladic lineament (Walcott and White, 1998), must be a tectonic boundary. To accommodate rotations at temperatures below the Curie temperature of the dominant magnetic carriers in our samples (magnetite), this structure must have acted at mid- to lower-greenschist facies and possibly to brittle conditions. This is corroborated by the succession of structures observed within the Marathi Unit and especially the pre-Alpine basement. Amphibolite-facies fabrics in the Marathi Unit are deformed by narrow mylonitic shear zones that are also parallel to the mylonitic fabric developed in broader zones in the basement orthogneisses, which in turn are overprinted by more brittle structures (shear bands, rotated tension gashes, cataclasites). Although earlier ductile fabrics between the metamorphic lithologies of the Marathi Unit and the pre-Alpine basement are parallel or subparallel to each other, occasionally, low-angle ductile shear zones and cataclastic fault zones crosscut the contact.

We infer such a low-angle shear zone that coincides with the tectonic contact between the metamorphic rocks of the northern domain, dominated by the structurally lower pre-Alpine basement, and the metamorphic rocks of the southern domain, dominated by the structurally higher Marathi Unit. This structure, here called the Elitas fault zone, is in present-day coordinates a low-angle, oblique, top-to-the-E, ductile-to-brittle normal fault dipping to the SE located more or less along the eastern flank of the Paroikia-Naoussa valley, and it probably continues to the SW. The strain on this fault was preferentially partitioned along the gneiss-marble boundary forming and overprinting mylonites and ultramylonites (Papanikolaou, 1980; Gautier et al., 1993). Although the major structures of Paros are described between the main lithological units, the Elitas fault zone must cut the (probably folded) contact between the Marathi Unit and the pre-Alpine basement: Both units are present in both the northern and southern domains.

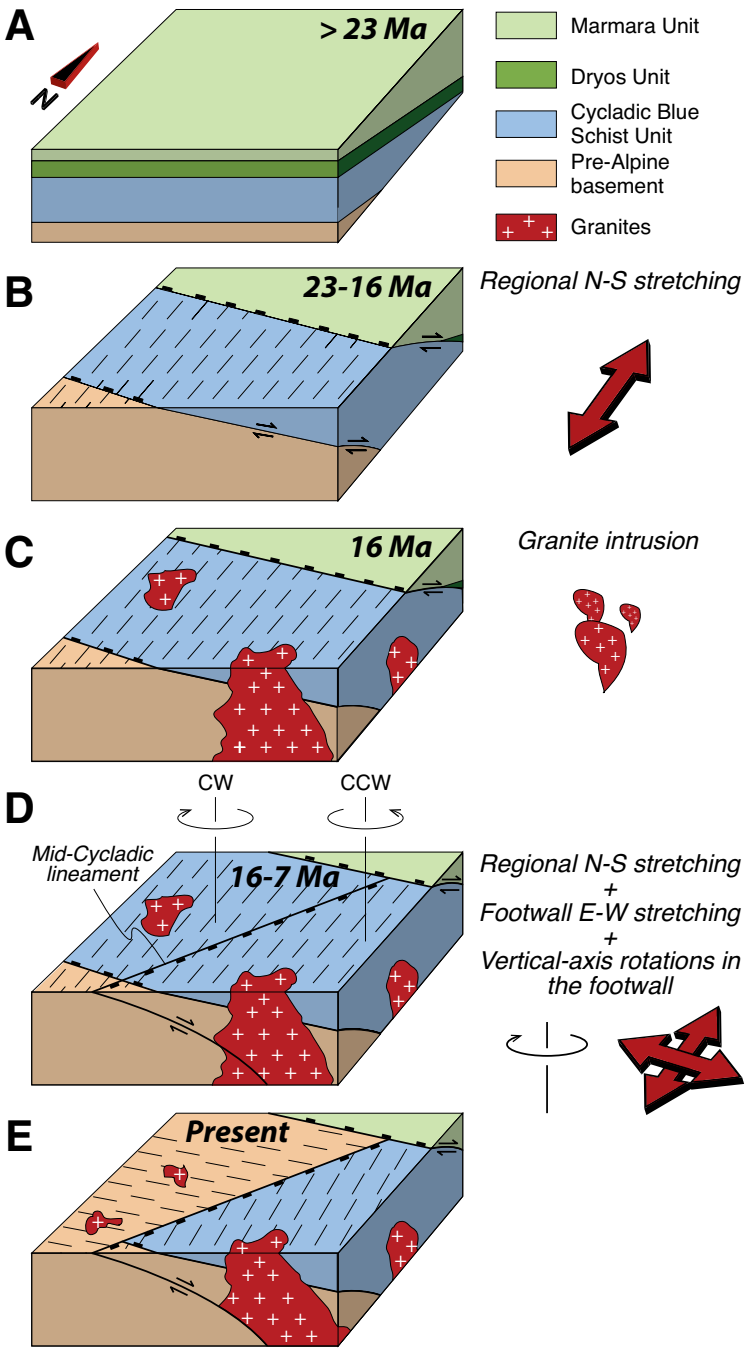

Figure 11. Three-dimensional (3-D) model for the synexhumation rotation history and detachment configuration of Paros Island. (A) Pre-extension nappe stacking configuration. (B) During stage 1, exhumation of basement orthogneisses and Marathi Unit from amphibolite to greenschist facies is accommodated along a top-to-the-N high-grade shear zone along the basement orthogneiss–Marathi Unit contact. Similar structures are also developed along the contact between the Marathi Unit and Dryos Unit. (C) During stage 2, basement orthogneisses and Marathi Unit have reached greenschist-facies structural levels, and the granitic rocks have intruded the basement and locally pierce through the basement orthogneiss–Marathi Unit contact. (D) During stage 3, northern and southern Paros become separated by the Elitas shear zone and undergo relative rotations. (E) Present-day configuration. CW—clockwise; CCW—counterclockwise.

We envisage the following tectonic history for the island of Paros. In the first stage, exhumation was accommodated along the detachment at the base of the Marmara Unit in latest Oligocene to Early Miocene time. This phase of exhumation brought the Dryos Unit, the Marathi Unit (Cycladic Blueschist Unit), and deeper units to greenschist-facies, midcrustal conditions prior to granitoid intrusion around 16 Ma. After 16 Ma, and prior to the arrival of the Marathi and deeper units to the surface shortly after 8 Ma (suggested by [U-Th]/He ages; Brichau et al., 2006; Bargnesi et al., 2013), the footwall to the Piso Livadi detachment broke into two blocks, which underwent opposite rotations, separated by the Elitas low-angle normal fault zone. The southern domain of Paros, in the hanging wall to the Elitas fault zone, continued exhumation along the Piso Livadi detachment, which led to the juxtaposition of the pre-Alpine basement against the Neogene sediments, whereas the northern domain underwent additional exhumation accommodated along the Elitas fault zone. Even though there is no demonstrable major metamorphic contrast between the hanging wall and footwall of the Elitas fault zone—both the pre-Alpine basement in the footwall and the Marathi Unit in the hanging wall experienced Early Miocene amphibolite-facies metamorphism—we consider the Elitas fault zone to be an extensional detachment fault that must have had considerable displacement, given the major vertical-axis rotation it accommodated (Fig. 11). Kinematic mechanisms other than the one proposed here are inconsistent with the observed geological evidence.

Implications for the Role of the Mid-Cycladic Lineament during Aegean Oroclinal Bending

The kinematic history of Paros Island closely mimics the regional pattern of vertical-axis rotations and extensional exhumation in the wider Aegean region. Van Hinsbergen and Schmid (2012), as well as Jolivet et al. (2015) and Brun et al. (2016), concluded that in a first stage of regional extension in Oligocene to Early Miocene time, until ca. 15 Ma, the Aegean domain was characterized by no more than 10° clockwise rotation accommodated by extensional detachments in the Rhodope mountains, western mainland Greece, the Cyclades, and the northern Menderes Massif. Van Hinsbergen (2010) and van Hinsbergen and Schmid (2012) argued that this rotation must have been accommodated along a left-lateral transform fault bounding the Menderes Massif to the east, which lies now buried below the Lycian Nappes of southwestern Turkey. During this stage, the exhumation of the Cycladic Blueschist Unit on Paros from amphibolite- to

greenschist-facies metamorphism must have occurred. In a second stage, starting around 15 Ma, rapid and opposite rotations occurred on both sides of the Aegean region. These rotations were as much as ~40° clockwise in western Greece and 20° counterclockwise in western Turkey (Fig. 2). The close correspondence of modern stretching lineation patterns with the amount of paleomagnetically documented rotation within these domains led van Hinsbergen and Schmid (2012) to argue that the southeastern Cycladic region was included in the counterclockwise-rotating domain, which is consistent with our paleomagnetic results from southern Paros.

Our analysis of Paros Island for the first time elucidates the tectonic nature of the only exposed contact between domains with strongly different stretching lineations in central Greece, interpreted as the Mid-Cycladic lineament: We demonstrate that, at least on Paros, this structure accommodates the vertical-axis rotation difference along a low-angle, top-to-the-E or -SE extensional structure. This is consistent with predictions from the kinematic restoration of van Hinsbergen and Schmid (2012), which indicated that the rotation difference between the northwestern and southeastern Aegean domains must have been accommodated along a structure that accommodated the trench-parallel lengthening of the Aegean orocline (i.e., and arc-parallel extensional structure), hitherto only demonstrated by E-W–trending stretching lineations associated with an extensional detachment on Samos Island (Ring et al., 1999; Fig. 2). We note, however, that the amount of clockwise rotation on northwestern Paros is some 30° more than the regional pattern, suggesting that local rotations also must have played a role on Paros. If Paros is representative of the Mid-Cycladic lineament, our results suggest that the southeastern Cycladic domain was in a hanging-wall position relative to the northwestern domain, i.e., opposite to the scenario speculated upon by van Hinsbergen and Schmid (2012). Importantly, the geology of Paros island provides no support for the presence of a strike-slip fault that would have accommodated the rotation differences in the Central Aegean region, as speculated by Walcott and White (1998), Philippon et al. (2012, 2014), Brun et al. (2016), and Menant et al. (2016). This, in combination with the absence of any evidence for ~300 km of trench-parallel shortening, as required in the scenarios of Jolivet et al. (2015), Brun et al. (2016), and Menant et al. (2016), suggests that the Cycladic region must have accommodated combined arc-parallel and arc-normal extension, similar to the "crustal attenuation" modeled by Gautier et al. (1999), but more localized. This would define the Aegean region as an extensional orocline (Fig. 1), although evidence for folding of the exhumed rocks and the detachments of the Cyclades in the late stages of orocline formation, in Late Miocene and younger time, has been reported (Gautier et al., 1993; Avigad et al., 2001; Lecomte et al., 2010), which may indicate that Anatolian extrusion, largely in the Pliocene, may have led to some orogen-parallel contraction in the heart of the Aegean orocline (Menant et al., 2013; Philippon et al., 2014). This would shift the mode of oroclinal bending to the "broken slats" combination of extensional and contractional oroclinal bending, although most, if not all, of the vertical-axis rotation had already taken place (van Hinsbergen et al., 2005b, 2010a).

Finally, we note that the change in rotation style in the Aegean region, from a "windshield wiper" to a "double saloon door" mode, around 15 Ma postdates the onset of the high-temperature overprint and the regional granitoid intrusion that affected the Cycladic region in Late Early Miocene time (Jolivet et al., 2015; Menant et al., 2016). During rotation, granitoid intrusion continued in the central Aegean region, which was explained by Jolivet et al. (2015) as the result of flow around the eastern Aegean slab edge during rapid southwestward roll-back driving the rotations. We note that the evidence for combined arc-parallel and arc-normal extension in the heart of the Aegean orocline at the junction of the oppositely rotating domains would have attenuated the central Aegean crust much more than in adjacent areas, consistent with the observation of Tirel et al. (2004), who noted that the Cycladic area is currently underlain by the thinnest crust in the Aegean–west Anatolian region. This enhanced attenuation may have added to the rise of asthenosphere and partial melting of crust and mantle, producing the Late Miocene magmatism, without, or in addition to, the envisaged mantle flow.

CONCLUSIONS

Regional patterns of stretching lineations in the Aegean region suggest that the paleomagnetically documented opposite rotations of the Aegean–west Anatolian orocline are bounded along a structural discontinuity known as the Mid-Cycladic lineament. To elucidate the tectonic nature of this debated structure, we paleomagnetically studied the vertical-axis rotation history of Paros Island, which is the only location where both stretching lineation trends are exposed, and where the tectonic nature of the enigmatic Mid-Cycladic lineament may be directly analyzed. To the northwest of the lineament, stretching lineations in 23–16 Ma amphibolite-facies metamorphic rocks trend approximately E-W, whereas to the southeast, these rocks contain N-S stretching lineations. To this end, we collected 160 paleomagnetic samples from 16 sites in 16 Ma granitoid bodies that intruded the pervasive foliation that hosts these stretching lineations in both domains. We conclude the following:

(1) AMS measurements in the granitoids demonstrate that these are essentially isotropic, and that the measured declinations are not influenced by a deformation-induced mineral preferred orientation.

(2) Our paleomagnetic data show that the vertical-axis rotation difference across the interpreted Mid-Cycladic lineament on Paros Island is proportional to the angle between the stretching lineations. The northwestern block with approximately E-W–trending stretching lineations rotated ~90° clockwise, and the southeastern block with N-S–trending stretching lineations rotated ~10° counterclockwise relative to stable Eurasia.

(3) During a first stage of exhumation between ca. 23 and 16 Ma, the metamorphic rocks of Paros were exhumed from amphibolite-facies to greenschist-facies conditions without internal rotation. This was accommodated along the top-to-the-N Piso Livadi detachment.

(4) Following 16 Ma granitoid intrusion, the Elitas low-angle normal fault zone developed at the boundary between the northwestern and southeastern domain. This structure, which coincides with the Mid-Cycladic lineament, accommodated the vertical-axis rotation difference, accommodating a component of orogen-parallel extension, in addition to the still-active Marmara detachment that accommodated orogen-normal extension.

(5) We, for the first time, demonstrate that the vertical-axis rotation differences in the Cyclades are accommodated by an extensional fault zone. This is consistent with geometric requirements, i.e., that arc-parallel extension must accommodate arc-normal back-arc extension in the development of the Aegean orocline. We do not see grounds to infer major orogen-parallel shortening to account for the Aegean oroclinal bending, and we demonstrate that on the island of Paros, the Mid-Cycladic lineament is not a transform fault.

ACKNOWLEDGMENTS

Malandri acknowledges funding through the Greek State Foundation (IKY) Scholarship (Master's International Scholarship [MIS] program: 457232); van Hinsbergen and Maffione acknowledge European Research Council (ERC) Starting Grant 306810 (Subduction Initiation Reconstructed from Neotethyan Kinematics [SINK]) to van Hinsbergen; and van Hinsbergen acknowledges funding through Netherlands Organization for Scientific Research (NWO) Vidi grant 864.11.004. The field work for this research was partially funded by the National and Kapodistrian University of Athens' Special Account of Research Grants 10812. We thank Cor Langereis

for discussion. We thank Uwe Ring, Bernhard Grasemann, and an anonymous reviewer for comments.

REFERENCES CITED

Altherr, R., Kreuzer, H., Wendt, I., Lenz, H., Wagner, G.A., Keller, J., Harre, W., and Hohndorf, A., 1982, A late Oligocene/early Miocene high temperature belt in the Attica Cycladic crystalline complex (SE Pelagonian, Greece): Geologisches Jahrbuch, v. E23, p. 97–164.

Andriessen, P.A.M., Banga, G., and Hebeda, E.H., 1987, Isotopic age study of pre-Alpine rocks in the basal units on Naxos, Sikinos and Ios, Greek Cyclades: Geologie en Mijnbouw, v. 66, p. 3–14.

Avigad, D., and Garfunkel, Z., 1991, Uplift and exhumation of high-pressure metamorphic terrains: The example of the Cycladic blueschist belt (Aegean Sea): Tectonophysics, v. 188, p. 357–372, doi:10.1016/0040-1951(91)90464-4.

Avigad, D., Ziv, A., and Garfunkel, Z., 2001, Ductile and brittle shortening, extension-parallel folds and maintenance of crustal thickness in the central Aegean (Cyclades, Greece): Tectonics, v. 20, p. 277–287, doi:10.1029/2000TC001190.

Bargnesi, E.A., Stockli, D.F., Mancktelow, N., and Soukis, K., 2013, Miocene core complex development and coeval supradetachment basin evolution of Paros, Greece: Insights from (U-Th)/He thermochronometry: Tectonophysics, v. 595–596, p. 165–182, doi:10.1016/j.tecto.2012.07.015.

Blake, M.C., Bonneau, M., Geyssant, J., Kienast, J.R., Lepvrier, C., Maluski, H., and Papanikolaou, D., 1981, A geologic reconnaissance of the Cycladic blueschist belt, Greece: Geological Society of America Bulletin, v. 92, p. 247–254, doi:10.1130/0016-7606(1981)92<247:AGROTC>2.0.CO;2.

Bögek, H., 1983, Stratigraphische und tektonische Verknüpfungen kontinentaler Sedimente des Neogens im Ägäis-Raum: Geologische Rundschau, v. 72, p. 771–813, doi:10.1007/BF01848344.

Bolhar, R., Ring, U., and Allen, C.M., 2010, An integrated zircon geochronological and geochemical investigation into the Miocene plutonic evolution of the Cyclades, Aegean Sea, Greece: Part 1. Geochronology: Contributions to Mineralogy and Petrology, v. 160, p. 719–742, doi:10.1007/s00410-010-0504-4.

Bolhar, R., Ring, U., Kemp, A.I.S., Whitehouse, M.J., Weaver, S.D., Woodhead, J.D., Uysal, I.T., and Turnbull, R., 2012, An integrated zircon geochronological and geochemical investigation into the Miocene plutonic evolution of the Cyclades, Aegean Sea, Greece: Part 2. Geochemistry: Contributions to Mineralogy and Petrology, v. 164, p. 915–933, doi:10.1007/s00410-012-0759-z.

Bonneau, M., 1982, Évolution géodynamique de l'arc égéen depuis le Jurassique supérieure jusquáu Miocène: Bulletin de la Société Géologique de France, v. 7, p. 229–242, doi:10.2113/gssgfbull.S7-XXIV.2.229.

Borradaile, G.J., 1991, Correlation of strain with anisotropy of magnetic susceptibility (AMS): Pure and Applied Geophysics, v. 135, p. 15–29, doi:10.1007/BF00877006.

Borradaile, G.J., 1988, Magnetic susceptibility, petrofabrics and strain: Tectonophysics, v. 156, p. 1–20, doi:10.1016/0040-1951(88)90279-X.

Bozkurt, E., and Satir, M., 2000, The southern Menderes Massif (western Turkey): Geochronology and exhumation history: Geological Journal, v. 35, no. 3-4, p. 285–296, doi:10.1002/gj.849.

Brichau, S., Ring, U., Ketcham, R.A., Carter, A., Stockli, D., and Brunel, M., 2006, Constraining the long-term evolution of the slip rate for a major extensional fault system in the central Aegean, Greece, using thermochronology: Earth and Planetary Science Letters, v. 241, p. 293–306, doi:10.1016/j.epsl.2005.09.065.

Bröcker, M., and Franz, L., 1998, Rb-Sr isotope studies on Tinos Island (Cyclades, Greece): Additional time constraints for metamorphism, extent of infiltration controlled overprinting and deformational activity: Geological Magazine, v. 135, p. 369–382, doi:10.1017/S0016756898008681.

Bröcker, M., and Franz, L., 2006, Dating metamorphism and tectonic juxtaposition on Andros Island (Cyclades, Greece): Results of a Rb-Sr study: Geological Magazine, v. 143, p. 609–620, doi:10.1017/S001675680600241X.

Bröcker, M., and Pidgeon, R.T., 2007, Protolith ages of metaigneous and metatuffaceous rocks from the Cycladic Blueschist Unit, Greece: Results of a reconnaissance U-Pb zircon study: The Journal of Geology, v. 115, p. 83–98, doi:10.1086/509269.

Bröcker, M., Kreuzer, H., Matthew, A., and Okrusch, M., 1993, $^{40}Ar/^{39}Ar$ and oxygen isotope studies of polymetamorphism from Tinos Island, Cycladic blueschist belt, Greece: Journal of Metamorphic Geology, v. 11, p. 223–240, doi:10.1111/j.1525-1314.1993.tb00144.x.

Brun, J.-P., and Faccenna, C., 2008, Exhumation of high-pressure rocks driven by slab rollback: Earth and Planetary Science Letters, v. 272, p. 1–7, doi:10.1016/j.epsl.2008.02.038.

Brun, J.-P., and Sokoutis, D., 2007, Kinematics of the Southern Rhodope core complex (northern Greece): International Journal of Earth Sciences, v. 96, p. 1079–1099, doi:10.1007/s00531-007-0174-2.

Brun, J.-P., and Sokoutis, D., 2010, 45 m.y. of Aegean crust and mantle flow driven by trench retreat: Geology, v. 38, p. 815–818, doi:10.1130/G30950.1.

Brun, J.-P., Faccenna, C., Gueydan, F., Sokoutis, D., Philippon, M., Kydonakis, K., and Gorini, C., 2016, The two-stage Aegean extension, from localized to distributed, a result of slab rollback acceleration: Canadian Journal of Earth Sciences (in press), doi:10.1139/cjes-2015-0203.

Buick, I.S., and Holland, T.J.B., 1989, The *P-T-t* path associated with crustal extension, Naxos, Cyclades, Greece, *in* Daly, J.S., Cliff, R.A., and Yardley, B.W.D., eds., Evolution of Metamorphic Belts: Geological Society, London, Special Publication 43, p. 365–369, doi:10.1144/GSL.SP.1989.043.01.32.

Carey, S.W., 1955, The orocline concept in geotectonics: Proceedings of the Royal Society of Tasmania, v. 89, p. 255–288.

Cavazza, W., Okay, A.I., and Zattin, M., 2009, Rapid early–middle Miocene exhumation of the Kazdağ Massif (western Anatolia): International Journal of Earth Sciences, v. 98, p. 1935–1947, doi:10.1007/s00531-008-0353-9.

Cifelli, F., Rossetti, F., Mattei, M., Hirt, A.M., Funiciello, R., and Tortorici, L., 2004, An AMS, structural and paleomagnetic study of Quaternary deformation in eastern Sicily: Journal of Structural Geology, v. 26, p. 29–46, doi:10.1016/S0191-8141(03)00092-0.

Cifelli, F., Mattei, M., Chadima, M., Hirt, A., and Hansen, A., 2005, The origin of tectonic lineation in extensional basins: Combined neutron texture and magnetic analyses on "undeformed" clays: Earth and Planetary Science Letters, v. 235, p. 62–78, doi:10.1016/j.epsl.2005.02.042.

Deenen, M.H.L., Langereis, C.G., van Hinsbergen, D.J.J., and Biggin, A.J., 2011, Geomagnetic secular variation and the statistics of palaeomagnetic directions: Geophysical Journal International, v. 186, p. 509–520, doi:10.1111/j.1365-246X.2011.05050.x.

de Leeuw, A., Mandic, O., Krijgsman, W., Kuiper, K.F., and Hrvatovic, H., 2012, Paleomagnetic and geochronologic constraints on the geodynamic evolution of the Central Dinarides: Tectonophysics, v. 530–531, p. 286–298, doi:10.1016/j.tecto.2012.01.004.

Diamantopoulos, A., Krohe, A., and Mposkos, E., 2009, Kinematics of conjugate shear zones, displacement partitioning and fragmentation of the upper rigid crust during denudation of high-*P* rocks (Pelagonian and Sub-Pelagonian zones, Greece): Tectonophysics, v. 473, p. 84–98, doi:10.1016/j.tecto.2008.05.028.

Durr, S., Seidel, E., Kreuzer, H., and Harre, W., 1978, Témoins dún métamorphisme d'âge crétacé supérieur dans l'Égéide: Datations radiométriques de minéraux provenant de l'île de Nikouriá (Cyclades, Grèce): Bulletin de la Société Géologique de France, v. 7, p. 209–213, doi:10.2113/gssgfbull.S7-XX.2.209.

Engel, M., and Reischmann, T., 1998, Single zircon geochronology of orthogneisses from Parox, Greece: Bulletin of the Geological Society of Greece, v. 22, p. 91–99.

Fisher, R.A., 1953, Dispersion on a sphere: Proceedings of the Royal Society of London, v. 217, p. 295–305, doi:10.1098/rspa.1953.0064.

Forster, M.A., and Lister, G.S., 1999, Detachment faults in the Aegean core complex of Ios, Cyclades, Greece, *in* Ring, U., Brandon, M.T., Lister, G.S., and Willett, S.D., eds., Exhumation Processes: Normal Faulting, Ductile Flow, and Erosion: Geological Society, London, Special Publication 154, p. 305–323, doi:10.1144/GSL.SP.1999.154.01.14.

Fytikas, M., Innocenti, F., Manetti, P., Peccerillo, A., Mazzuoli, R., and Villari, L., 1984, Tertiary to Quaternary evolution of volcanism in the Aegean region, *in* Dixon, J.E., and Robertson, A.H.F., eds., The Geological Evolution of the Eastern Mediterranean: Geological Society, London, Special Publication 17, p. 687–699, doi:10.1144/GSL.SP.1984.017.01.55.

Gautier, P., and Brun, J.P., 1994, Ductile crust exhumation and extensional detachments in the central Aegean (Cyclades and Evvia Islands): Geodinamica Acta, v. 7, p. 57–85, doi:10.1080/09853111.1994.11105259.

Gautier, P., Brun, J.-P., and Jolivet, L., 1993, Structure and kinematics of Upper Cenozoic extensional detachment on Naxos and Paros (Cyclades Islands, Greece): Tectonics, v. 12, p. 1180–1194, doi:10.1029/93TC01131.

Gautier, P., Brun, J.P., Moriceau, R., Sokoutis, D., and Martinod, J., 1999, Timing, kinematics and cause of Aegean extension: A scenario based on a comparison with simple analogue experiments: Tectonophysics, v. 315, p. 31–72, doi:10.1016/S0040-1951(99)00281-4.

Gradstein, F.M., Ogg, J.G., Schmitz, M., and Ogg, G., 2012, The Geologic Time Scale 2012: Amsterdam, Netherlands, Elsevier, 1175 p.

Grasemann, B., Schneider, D.A., Stockli, D.F., and Iglseder, C., 2012, Miocene bivergent crustal extension in the Aegean: Evidence from the western Cyclades (Greece): Lithosphere, v. 4, p. 23–39, doi:10.1130/L164.1.

Hetzel, R., Passchier, C.W., Ring, U., and Dora, O.O., 1995, Bivergent extension in orogenic belts: The Menderes Massif (southwestern Turkey): Geology, v. 23, p. 455–458, doi:10.1130/0091-7613(1995)023<0455:BEIOBT>2.3.CO;2.

Horner, F., and Freeman, R., 1982, Preliminary palaeomagnetic results from the Ionian zone, western Greece: EOS, v. 63, p. 1273.

Horner, F., and Freeman, R., 1983, Palaeomagnetic evidence from pelagic limestones for clockwise rotation of the Ionian zone, western Greece: Tectonophysics, v. 98, p. 11–27, doi:10.1016/0040-1951(83)90208-1.

Hrouda, F., 1982, Magnetic anisotropy of rocks and its applicability in geology and geophysics: Geophysical Surveys, v. 5, p. 37–82, doi:10.1007/BF01450244.

Hrouda, F., 1993, Theoretical models of magnetic anisotropy to strain relationship revisited: Physics of the Earth and Planetary Interiors, v. 77, p. 237–249, doi:10.1016/0031-9201(93)90101-E.

Hubert-Ferrari, A., Armijo, R., King, G., Meyer, B., and Barka, A., 2002, Morphology, displacement, and slip rates along the North Anatolian fault, Turkey: Journal of Geophysical Research, v. 107, no. B10, p. 2235, doi:10.1029/2001JB000393.

Hubert-Ferrari, A., King, G., van der Woerd, J., Villa, I., Altunel, E., and Armijo, R., 2009, Long-term evolution of the North Anatolian fault: New constraints from its eastern termination, *in* van Hinsbergen, D.J.J., Edwards, M.A., and Govers, R., eds., Collision and Collapse at the Africa-Arabia-Eurasia Subduction Zone: Geological Society, London, Special Publication 311, p. 133–154, doi:10.1144/SP311.5.

Huet, B., Labrousse, L., and Jolivet, L., 2009, Thrust or detachment? Exhumation processes in the Aegean: Insight from a field study on Ios (Cyclades, Greece): Tectonics, v. 28, TC3007, doi:10.1029/2008TC002397.

Iglseder, C., Grasemann, B., Rice, A.H.N., Petrakakis, K., and Schneider, D.A., 2011, Miocene south directed low-angle normal fault evolution on Kea Island (West Cycladic detachment system, Greece): Tectonics, v. 30, TC4013, doi:10.1029/2010TC002802.

Işık, V., and Tekeli, O., 2001, Late orogenic crustal extension in the northern Menderes Massif (western Turkey): Evidence for metamorphic core complex formation: International Journal of Earth Sciences, v. 89, p. 757–765, doi:10.1007/s005310000105.

Işık, V., Seyitoglu, G., and Cemen, I., 2003, Ductile-brittle transition along the Alaşehir detachment fault and its structural relationship with the Simav detachment fault, Menderes Massif, western Turkey: Tectonophysics, v. 374, p. 1–18, doi:10.1016/S0040-1951(03)00275-0.

Işık, V., Tekeli, O., and Seyitoglu, G., 2004, The $^{40}Ar/^{39}Ar$ age of extensional ductile deformation and granitoid intrusion in the northern Menderes core complex: Implications for the initiation of extensional tectonics in western Turkey: Journal of Asian Earth Sciences, v. 23, p. 555–566, doi:10.1016/j.jseaes.2003.09.001.

Jansen, J.B.H., and Schuiling, R.D., 1976, Metamorphism on Naxos; petrology and geothermal gradients: American

Journal of Science, v. 276, p. 1225–1253, doi:10.2475/ajs.276.10.1225.
Jelínek, V., 1977, The statistical Theory of Measuring Anisotropy of Magnetic Susceptibility of Rocks and its Application: Brno, Czechoslovakia, Geofyzika n.p., 87 p.
Jelínek, V., 1981, Characterization of the magnetic fabrics of rocks: Tectonophysics, v. 79, p. 63–67, doi:10.1016/0040-1951(81)90110-4.
Jelínek, V., and Kropácek, V., 1978, Statistical processing of anisotropy of magnetic susceptibility measured on groups of specimens: Studia Geophysica et Geodaetica, v. 22, p. 50–62, doi:10.1007/BF01613632.
Johnson, C.L., Constable, C.G., Tauxe, L., Barendregt, R., Brown, L.L., Coe, R.S., Layer, P., Mejia, V., Opdyke, N.D., Singer, B.S., Staudigel, H., and Stone, D.B., 2008, Recent investigations of the 0–5 Ma geomagnetic field recorded by lava flows: Geochemistry, Geophysics, Geosystems, v. 9, p. Q04032, doi:10.1029/2007GC001696.
Johnston, S.T., 2001, The Great Alaskan terrane wreck: Reconciliation of paleomagnetic and geological data in the Northern Cordillera: Earth and Planetary Science Letters, v. 193, p. 259–272, doi:10.1016/S0012-821X(01)00516-7.
Jolivet, L., 2001, A comparison of geodetic and finite strain pattern in the Aegean, geodynamic implications: Earth and Planetary Science Letters, v. 187, p. 95–104, doi:10.1016/S0012-821X(01)00277-1.
Jolivet, L., and Brun, J.-P., 2010, Cenozoic geodynamic evolution of the Aegean: International Journal of Earth Sciences, v. 99, p. 109–138, doi:10.1007/s00531-008-0366-4.
Jolivet, L., Goffé, B., Monié, P., Truffert-Luxey, C., Patriat, M., and Bonneau, M., 1996, Miocene detachment in Crete and exhumation *P-T-t* paths of high-pressure metamorphic rocks: Tectonics, v. 15, p. 1129–1153, doi:10.1029/96TC01417.
Jolivet, L., Lecomte, E., Huet, B., Denèle, Y., Lacombe, O., Labrousse, L., Le Pourhiet, L., and Mehl, C., 2010a, The North Cycladic detachment system: Earth and Planetary Science Letters, v. 289, p. 87–104, doi:10.1016/j.epsl.2009.10.032.
Jolivet, L., Labrousse, L., Agard, P., Lacombe, O., Bailly, V., Lecomte, E., Mouthereau, F., and Mehl, C., 2010b, Rifting and shallow-dipping detachments, clues from the Corinth Rift and the Aegean: Tectonophysics, v. 483, p. 287–304, doi:10.1016/j.tecto.2009.11.001.
Jolivet, L., Faccenna, C., Huet, B., and Labrousse, L., 2013, Aegean tectonics: Strain localisation, slab tearing and trench retreat: Tectonophysics, v. 597–598, p. 1–33, doi:10.1016/j.tecto.2012.06.011.
Jolivet, L., Menant, A., Sternai, P., Rabillard, A., Arbaret, L., Augier, R., Laurent, V., Beaudoin, A., Grasemann, B., Huet, B., Labrousse, L., and Le Pourhiet, L., 2015, The geological signature of a slab tear below the Aegean: Tectonophysics, v. 659, p. 166–182, doi:10.1016/j.tecto.2015.08.004.
Keay, S., Lister, G., and Buick, I., 2001, The timing of partial melting, Barrovian metamorphism and granite intrusion in the Naxos metamorphic core complex, Cyclades, Aegean Sea, Greece: Tectonophysics, v. 342, p. 275–312, doi:10.1016/S0040-1951(01)00168-8.
Kirschvink, J.L., 1980, The least-squares line and plane and the analysis of palaeomagnetic data: Geophysical Journal of the Royal Astrological Society, v. 62, p. 699–718, doi:10.1111/j.1365-246X.1980.tb02601.x.
Kisch, H.J., 1981, Burial diagenesis in Tertiary "flysch" of the external zones of the Hellenides in central Greece and the Olympos region, and its tectonic significance: Eclogae Geologicae Helvetiae, v. 74, p. 603–624.
Kissel, C., and Laj, C., 1988, The Tertiary geodynamical evolution of the Aegean arc: A paleomagnetic reconstruction: Tectonophysics, v. 146, p. 183–201, doi:10.1016/0040-1951(88)90090-X.
Kissel, C., and Poisson, A., 1987, Étude paléomagnetique préliminaire des formations cénozoïques des Bey Daglari (Taurides occidentales, Turquie): Comptes Rendus Académie Science Paris, v. 304, ser. II, p. 343–348.
Kissel, C., Laj, C., and Jamet, M., 1984, Palaeomagnetic evidence of Miocene and Pliocene rotational deformations of the Aegean area, *in* Dixon, J.E., and Robertson, A.H.F., eds., The Geological Evolution of the Eastern Mediterranean: Geological Society, London, Special Publication 17, p. 669–679, doi:10.1144/GSL.SP.1984.017.01.53.
Kissel, C., Laj, C., and Müller, C., 1985, Tertiary geodynamical evolution of northwestern Greece: Paleomagnetic results: Earth and Planetary Science Letters, v. 72, p. 190–204, doi:10.1016/0012-821X(85)90005-6.
Kissel, C., Laj, C., Şengör, A.M.C., and Poisson, A., 1987, Paleomagnetic evidence for rotation in opposite senses of adjacent blocks in northeastern Aegean and western Anatolia: Geophysical Research Letters, v. 14, p. 907–910, doi:10.1029/GL014i009p00907.
Kissel, C., Laj, C., Poisson, A., and Simeakis, K., 1989, A pattern of block rotations in central Aegean, *in* Kissel, C., and Laj, C., eds., Paleomagnetic Rotations and Continental Deformation: Dordrecht, Netherlands, Springer p. 115–129.
Kissel, C., Speranza, F., and Milicevic, V., 1995, Paleomagnetism of external southern and central Dinarides and northern Albanides: Implications for the Cenozoic activity of the Scutari-Pec transverse zone: Journal of Geophysical Research, v. 100, p. 14,999–15,007, doi:10.1029/95JB01243.
Koymans, M.R., Langereis, C.G., Pastor-Galan, D., and van Hinsbergen, D.J.J., 2016, Paleomagnetism.org: An online multi-platform open source environment for paleomagnetic data analysis: Computers & Geosciences, v. 93, p. 127–137.
Lecomte, E., Jolivet, L., Lacombe, O., Denèle, Y., Labrousse, L., and Le Pourhiet, L., 2010, Geometry and kinematics of Mykonos detachment, Cyclades, Greece: Evidence for slip at shallow dip: Tectonics, v. 29, TC5012, doi:10.1029/2009TC002564.
Le Pichon, X., and Angelier, J., 1981, The Aegean Sea: Philosophical Transactions of the Royal Society of London, v. 300, p. 357–372, doi:10.1098/rsta.1981.0069.
Le Pichon, X., Şengör, A.M.C., Kende, J., Imren, C., Henry, P., Grall, C., and Karabulut, H., 2016, Propagation of a strike-slip plate boundary within an extensional environment: The westward propagation of the North Anatolian fault: Canadian Journal of Earth Sciences (in press), doi:10.1139/cjes-2015-0129.
Li, P., Rosenbaum, G., and Donchak, P.J.T., 2012, Structural evolution of the Texas orocline, eastern Australia: Gondwana Research, v. 22, p. 279–289, doi:10.1016/j.gr.2011.09.009.
Lips, A.L.W., Cassard, D., Sözbilir, H., Yilmaz, H., and Wijbrans, J.R., 2001, Multistage exhumation of the Menderes Massif, western Anatolia (Turkey): International Journal of Earth Sciences, v. 89, p. 781–792, doi:10.1007/s005310000101.
Lister, G., Banga, G., and Feenstra, A., 1984, Metamorphic core complexes of Cordilleran type in the Cyclades. Aegean Sea, Greece: Geology, v. 12, p. 221–225, doi:10.1130/0091-7613(1984)12<221:MCCOCT>2.0.CO;2.
Maffione, M., Speranza, F., and Faccenna, C., 2009, Bending of the Bolivian orocline and growth of the Central Andean Plateau: Paleomagnetic and structural constraints from the Eastern Cordillera (22–24°S, NW Argentina): Tectonics, v. 28, TC4006, doi:10.1029/2008TC002402.
Maffione, M., Pucci, S., Sagnotti, L., and Speranza, F., 2012, Magnetic fabric of Pleistocene continental clays from the hanging-wall of an active low-angle normal fault (Altotiberina fault, Italy): International Journal of Earth Sciences, v. 101, p. 849–861, doi:10.1007/s00531-011-0704-9.
Maffione, M., Hernandez-Moreno, C., Ghiglione, M.C., Speranza, F., van Hinsbergen, D.J.J., and Lodolo, E., 2015, Constraints on deformation of the Southern Andes since the Cretaceous from anisotropy of magnetic susceptibility: Tectonophysics, v. 665, p. 236–250, doi:10.1016/j.tecto.2015.10.008.
Marsellos, A.E., and Kidd, W.S.F., 2008, Extension and exhumation of the Hellenic forearc ridge in Kythera: The Journal of Geology, v. 116, p. 640–651, doi:10.1086/591995.
Marshak, S., 1988, Kinematics of orocline and arc formation in thin-skinned orogens: Tectonics, v. 7, p. 73–86, doi:10.1029/TC007i001p00073.
Mattei, M., Sagnotti, L., Faccenna, C., and Funiciello, R., 1997, Magnetic fabric of weakly deformed clay-rich sediments in the Italian peninsula: Relationship with compressional and extensional tectonics: Tectonophysics, v. 271, p. 107–122, doi:10.1016/S0040-1951(96)00244-2.
Mattei, M., Speranza, F., Argentieri, A., Rossetti, F., Sagnotti, L., and Funiciello, R., 1999, Extensional tectonics in the Amantea basin (Calabria, Italy): A comparison between structural and magnetic anisotropy data: Tectonophysics, v. 307, p. 33–49, doi:10.1016/S0040-1951(99)00117-1.
Mauritsch, H.J., Scholger, R., Bushati, S.L., and Ramiz, H., 1995, Palaeomagnetic results from southern Albania and their significance for the geodynamic evolution of the Dinarides, Albanides and Hellenides: Tectonophysics, v. 242, p. 5–18, doi:10.1016/0040-1951(94)00150-8.
Mauritsch, H.J., Scholger, R., Bushati, S.L., and Xhomo, A., 1996, Palaeomagnetic investigations in northern Albania and their significance for the geodynamic evolution of the Adriatic-Aegean realm, *in* Morris, A., and Tarling, D.H., eds., Palaeomagnetism and Tectonics of the Mediterranean Region: Geological Society, London, Special Publication 105, p. 265–275, doi:10.1144/GSL.SP.1996.105.01.23.
Menant, A., Jolivet, L., Augier, R., and Skarpelis, N., 2013, The North Cycladic detachment system and associated mineralization, Mykonos, Greece: Insights on the evolution of the Aegean domain: Tectonics, v. 32, p. 433–452, doi:10.1002/tect.20037.
Menant, A., Jolivet, L., and Vrielynck, B., 2016, Kinematic reconstructions and magmatic evolution illuminating crustal and mantle dynamics of the Eastern Mediterranean region since the Late Cretaceous: Tectonophysics, v. 675, p. 103–140, doi:10.1016/j.tecto.2016.03.007.
Morris, A., 1995, Rotational deformation during Palaeogene thrusting and basin closure in eastern central Greece: Palaeomagnetic evidence from Mesozoic carbonates: Geophysical Journal International, v. 121, p. 827–847, doi:10.1111/j.1365-246X.1995.tb06442.x.
Morris, A., and Anderson, M., 1996, First palaeomagnetic results from the Cycladic Massif, Greece, and their implications for Miocene extension directions and tectonic models in the Aegean: Earth and Planetary Science Letters, v. 142, p. 397–408, doi:10.1016/0012-821X(96)00114-8.
Morris, A., and Robertson, A., 1993, Miocene remagnetisation of carbonate platform and Antalya complex units within the Isparta Angle, SW Turkey: Tectonophysics, v. 220, p. 243–266, doi:10.1016/0040-1951(93)90234-B.
Mullender, T., Van Velzen, A.J., and Dekkers, M.J., 1993, Continuous drift correction and separate identification of ferrimagnetic and paramagnetic contributions in thermomagnetic runs: Geophysical Journal International, v. 114, p. 663–672, doi:10.1111/j.1365-246X.1993.tb06995.x.
Okay, A.I., 2001, Stratigraphic and metamorphic inversions in the central Menderes Massif: A new structural model: International Journal of Earth Sciences, v. 89, p. 709–727, doi:10.1007/s005310000098.
Okrusch, M., and Bröcker, M., 1990, Eclogite facies rocks in the Cycladic blueschist belt, Greece: A review: European Journal of Mineralogy, v. 2, p. 451–478.
Papanikolaou, D., 1977, On the structural geology and tectonics of Paros Island (Aegean Sea): Annales Géologiques des Pays Helléniques, v. 28, p. 450–463.
Papanikolaou, D., 1980, Contribution of the geology of the Aegean Sea: Annales Géologiques des Pays Helléniques, v. 30, p. 65–93.
Papanikolaou, D.J., 1987, Tectonic evolution of the Cycladic blueschist belt (Aegean Sea, Greece), *in* Helgeson, H.C., ed., Chemical Transport in Metasomatic Processes: Dordrecht, Netherlands, Springer p. 429–450.
Papanikolaou, D., 1996, Geological Map of Paros: Athens, Greece, Institute of Geology and Mineral Exploration, scale: 1:50,000.
Parés, J.M., van der Pluijm, B.A., and Dinares-Turell, J., 1999, Evolution of magnetic fabrics during incipient deformation of mudrocks (Pyrenees, northern Spain): Tectonophysics, v. 307, p. 1–14, doi:10.1016/S0040-1951(99)00115-8.
Pastor-Galan, D., Groenewegen, T., Brouwer, D., Krijgsman, W., and Dekkers, M.J., 2015, One or two oroclines in the Variscan orogen of Iberia? Implications for Pangea amalgamation: Geology, v. 43, p. 527–530, doi:10.1130/G36701.1.
Pastor-Galán, D., Mulchrone, K.F., Koymans, M.R., van Hinsbergen, D.J.J., and Langereis, C.G., 2016, Total least squares orocline test: A robust method to quantify vertical axis rotation patterns in orogens, with examples from the Cantabrian and Aegean oroclines: Lithosphere, doi:10.1130/L547.1 (in press).
Philippon, M., Brun, J.-P., and Gueydan, F., 2012, Deciphering subduction from exhumation in the segmented Cycladic Blueschist Unit (Central Aegean, Greece): Tectonophysics, v. 524–525, p. 116–134, doi:10.1016/j.tecto.2011.12.025.
Philippon, M., Brun, J.-P., Gueydan, F., and Sokoutis, D., 2014, The interaction between Aegean back-arc extension and Anatolia escape since Middle Miocene: Tectonophysics, v. 631, p. 176–188, doi:10.1016/j.tecto.2014.04.039.

Rimmelé, G., Oberhänsli, R., Goffé, B., Jolivet, L., Candan, O., and Cetinkaplan, M., 2003, First evidence of high-pressure metamorphism in the "Cover Series" of the southern Menderes Massif: Tectonic and metamorphic implications for the evolution of SW Turkey: Lithos, v. 71, p. 19–46, doi:10.1016/S0024-4937(03)00089-6.

Ring, U., Layer, P.W., and Reischmann, T., 2001, Miocene high-pressure metamorphism in the Cyclades and Crete, Aegean Sea, Greece: Evidence for large-magnitude displacement on the Cretan detachment: Geology, v. 29, p. 395–398, doi:10.1130/0091-7613(2001)029<0395:MHPMIT>2.0.CO;2.

Ring, U., Laws, S., and Bernet, M., 1999, Structural analysis of a complex nappe sequence and late- orogenic basins from the Aegean Island of Samos, Greece: Journal of Structural Geology, v. 21, p. 1575–1601.

Ring, U., Thomson, S.N., and Bröcker, M., 2003, Fast extension but little exhumation: The Vari detachment in the Cyclades, Greece: Geological Magazine, v. 140, p. 245–252, doi:10.1017/S0016756803007799.

Ring, U., Glodny, J., Will, T., and Thomson, S.N., 2007a, An Oligocene extrusion wedge of blueschist-facies nappes on Evia, Aegean Sea, Greece: Implications for the early exhumation of high-pressure rocks: Journal of the Geological Society, London,, v. 164, p. 637–652, doi:10.1144/0016-76492006-041.

Ring, U., Will, T., Glodny, J., Kumerics, C., Gessner, K., Thomson, S., Güngör, T., Monié, P., Okrusch, M., and Drüppel, K., 2007b, Early exhumation of high-pressure rocks in extrusion wedges: The Cycladic Blueschist Unit in the eastern Aegean, Greece and Turkey: Tectonics, v. 26, TC2001, doi:10.1029/2005TC001872.

Ring, U., Glodny, J., Will, T., and Thomson, S.N., 2010, The Hellenic subduction system: High-pressure metamorphism, exhumation, normal faulting, and large-scale extension: Annual Review of Earth and Planetary Sciences, v. 38, p. 45–76, doi:10.1146/annurev.earth.050708.170910.

Ring, U., Glodny, J., Will, T., and Thomson, S.N., 2011, Normal faulting on Sifnos and the South Cycladic detachment system, Aegean Sea, Greece: Journal of the Geological Society, London, v. 168, p. 751–768, doi:10.1144/0016-76492010-064.

Robert, E., 1982, Contribution à l'Étude Géologique des Cyclades Grèce: l'Ile de Paros [These 3eme cycle]: Orsay, France, Universite de Paris-Sud (Orsay), 103 p.

Rosenbaum, G., Ring, U., and Kühn, A., 2007, Tectonometamorphic evolution of high-pressure rocks from the island of Amorgos (central Aegean, Greece): Journal of the Geological Society, London, v. 164, p. 425–438, doi:10.1144/0016-76492006-005.

Royden, L., 1993, The tectonic expression of slab pull at continental convergent boundaries: Tectonics, v. 12, p. 303–325, doi:10.1029/92TC02248.

Sagnotti, L., Faccenna, C., and Funiciello, R., 1994, Magnetic fabric and structural setting of Plio-Pleistocene clayey units in an extensional regime: The Tyrrhenian margin of central Italy: Journal of Structural Geology, v. 16, p. 1243–1257, doi:10.1016/0191-8141(94)90067-1.

Sánchez-Gómez, M., Avigad, D., and Heimann, A., 2002, Geochronology of clasts in allochthonous Miocene sedimentary sequences on Mykonos and Paros Islands: Implications for back-arc extension in the Aegean Sea: Journal of the Geological Society, London, v. 159, p. 45–60, doi:10.1144/0016-764901031.

Schliestedt, M., and Matthews, A., 1987, Transformation of blueschist to greenschist facies rocks as a consequence of fluid infiltration, Sifnos (Cyclades), Greece: Contributions to Mineralogy and Petrology, v. 97, p. 237–250, doi:10.1007/BF00371243.

Şengör, A.M.C., Tüysüz, O., Imren, C., Sakınç, M., Eyidogan, H., Görür, N., Le Pichon, X., and Rangin, C., 2005, The North Anatolian fault: A new look: Annual Review of Earth and Planetary Sciences, v. 33, p. 37–112, doi:10.1146/annurev.earth.32.101802.120415.

Sokoutis, D., Brun, J.P., Van den Driessche, J., and Pavlides, S., 1993, A major Oligo-Miocene detachment in southern Rhodope controlling north Aegean extension: Journal of the Geological Society, London,, v. 150, p. 243–246, doi:10.1144/gsjgs.150.2.0243.

Soukis, K., and Stockli, D.F., 2013, Structural and thermochronometric evidence for multistage exhumation of southern Syros, Cycladic islands, Greece: Tectonophysics, v. 595–596, p. 148–164, doi:10.1016/j.tecto.2012.05.017.

Speranza, F., Kissel, C., Islami, I., Hyseni, A., and Laj, C., 1992, First paleomagnetic evidence for rotation of the Ionian zone of Albania: Geophysical Research Letters, v. 19, p. 697–700, doi:10.1029/92GL00575.

Speranza, F., Islami, I., Kissel, C., and Hyseni, A., 1995, Palaeomagnetic evidence for Cenozoic clockwise rotation of the external Albanides: Earth and Planetary Science Letters, v. 129, p. 121–134.

Speranza, F., Sagnotti, L., and Mattei, M., 1997, Tectonics of the Umbria-Marche-Romagna Arc (central Northern Apennines, Italy): New paleomagnetic constraints: Journal of Geophysical Research, v. 102, p. 3153–3166, doi:10.1029/96JB03116.

Stouraiti, C., Mitropoulos, P., Tarney, J., Barreiro, B., McGrath, A.M., and Baltatzis, E., 2010, Geochemistry and petrogenesis of late Miocene granitoids, Cyclades, southern Aegean: Nature of source components: Lithos, v. 114, p. 337–352, doi:10.1016/j.lithos.2009.09.010.

Taymaz, T., Jackson, J., and McKenzie, D., 1991, Active tectonics of the north and central Aegean Sea: Geophysical Journal International, v. 106, p. 433–490, doi:10.1111/j.1365-246X.1991.tb03906.x.

Thomson, S.N., Ring, U., Brichau, S., Glodny, J., and Will, T.M., 2009, Timing and nature of formation of the Ios metamorphic core complex, southern Cyclades, Greece, *in* Ring, U., and Wernicke, B., eds., Extending a Continent: Architecture, Rheology, and Heat Budget: Geological Society, London, Special Publication 321, p. 139–167, doi:10.1144/SP321.7.

Tirel, C., Gueydan, F., Tiberi, C., and Brun, J.-P., 2004, Aegean crustal thickness inferred from gravity inversion: Geodynamical implications: Earth and Planetary Science Letters, v. 228, p. 267–280, doi:10.1016/j.epsl.2004.10.023.

Tirel, C., Gautier, P., van Hinsbergen, D.J.J., and Wortel, M.J.R., 2009, Sequential development of interfering metamorphic core complexes: Numerical experiments and comparison with the Cyclades, Greece, *in* van Hinsbergen, D.J.J., Edwards, M.A., and Govers, R., eds., Collision and Collapse at the Africa-Arabia-Eurasia Subduction Zone: Geological Society, London, Special Publication 311, p. 257–292, doi:10.1144/SP311.10.

Torsvik, T.H., Van der Voo, R., Preeden, U., MacNiocaill, C., Steinberger, B., Doubrovine, P.V., van Hinsbergen, D.J.J., Domeier, M., Gaina, C., Tohver, E., Meert, J.G., McCausland, P.J.A., and Cocks, L.R.M., 2012, Phanerozoic polar wander, palaeogeography and dynamics: Earth-Science Reviews, v. 114, p. 325–368, doi:10.1016/j.earscirev.2012.06.007.

van Hinsbergen, D.J.J., 2010, A key extensional metamorphic complex reviewed and restored: The Menderes Massif of western Turkey: Earth-Science Reviews, v. 102, p. 60–76, doi:10.1016/j.earscirev.2010.05.005.

van Hinsbergen, D.J.J., and Boekhout, F., 2009, Neogene brittle detachment faulting on Kos (E Greece): Implications for a southern break-away fault of the Menderes metamorphic core complex (western Turkey), *in* van Hinsbergen, D.J.J., Edwards, M.A., and Govers, R., eds., Collision and Collapse at the Africa-Arabia-Eurasia Subduction Zone: Geological Society, London, Special Publication 311, p. 311–320, doi:10.1144/SP311.12.

van Hinsbergen, D.J.J., and Schmid, S.M., 2012, Map view restoration of Aegean–west Anatolian accretion and extension since the Eocene: Tectonics, v. 31, TC5005, doi:10.1029/2012TC003132.

van Hinsbergen, D.J.J., Hafkenscheid, E., Spakman, W., Meulenkamp, J.E., and Wortel, M.J.R., 2005a, Nappe stacking resulting from subduction of oceanic and continental lithosphere below Greece: Geology, v. 33, p. 325–328, doi:10.1130/G20878.1.

van Hinsbergen, D.J.J., Langereis, C.G., and Meulenkamp, J.E., 2005b, Revision of the timing, magnitude and distribution of Neogene rotations in the western Aegean region: Tectonophysics, v. 396, p. 1–34, doi:10.1016/j.tecto.2004.10.001.

van Hinsbergen, D.J.J., Zachariasse, W.J., Wortel, M.J.R., and Meulenkamp, J.E., 2005c, Underthrusting and exhumation: A comparison between the External Hellenides and the "hot" Cycladic and "cold" South Aegean core complexes (Greece): Tectonics, v. 24, TC2011, doi:10.1029/2004TC001692.

van Hinsbergen, D.J.J., Dupont-Nivet, G., Nakov, R., Oud, K., and Panaiotu, C., 2008, No significant post-Eocene rotation of the Moesian Platform and Rhodope (Bulgaria): Implications for the kinematic evolution of the Carpathian and Aegean arcs: Earth and Planetary Science Letters, v. 273, p. 345–358, doi:10.1016/j.epsl.2008.06.051.

van Hinsbergen, D.J.J., Dekkers, M.J., and Koç, A., 2010a, Testing Miocene remagnetization of Bey Dağları: Timing and amount of Neogene rotations in SW Turkey: Turkish Journal of Earth Sciences, v. 19, p. 123–156.

van Hinsbergen, D.J.J., Dekkers, M.J., Bozkurt, E., and Koopman, M., 2010b, Exhumation with a twist: Paleomagnetic constraints on the evolution of the Menderes metamorphic core complex (western Turkey): Tectonics, v. 29, TC3009, doi:10.1029/2009TC002596.

van Hinsbergen, D.J.J., Kaymakci, N., Spakman, W., and Torsvik, T.H., 2010c, Reconciling the geological history of western Turkey with plate circuits and mantle tomography: Earth and Planetary Science Letters, v. 297, p. 674–686, doi:10.1016/j.epsl.2010.07.024.

van Hinsbergen, D.J.J., Mensink, M., Langereis, C.G., Maffione, M., Spalluto, L., Tropeano, M., and Sabato, L., 2014, Did Adria rotate relative to Africa?: Solid Earth, v. 5, p. 611–629, doi:10.5194/se-5-611-2014.

Walcott, C.R., and White, S.H., 1998, Constraints on the kinematics of post-orogenic extension imposed by stretching lineations in the Aegean region: Tectonophysics, v. 298, p. 155–175, doi:10.1016/S0040-1951(98)00182-6.

Weil, A.B., 2006, Kinematics of orocline tightening in the core of an arc: Paleomagnetic analysis of the Ponga Unit, Cantabrian Arc, northern Spain: Tectonics, v. 25, TC3012, doi:10.1029/2005TC001861.

Weil, A.B., and Sussman, A.J., 2004, Classifying curved orogens based on timing relationships between structural development and vertical-axis rotations, *in* Weil, A.B., and Sussman, A.J., eds., Orogenic Curvature: Integrating Paleomagnetic and Structural Analyses: Geological Society of America Special Paper 383, p. 1–15.

Wijbrans, J.R., Schliestedt, M., and York, D., 1990, Single grain argon laser probe dating of phengites from the blueschist to greenschist transition on Sifnos (Cyclades, Greece): Contributions to Mineralogy and Petrology, v. 104, p. 582–593, doi:10.1007/BF00306666.

Yonkee, A., and Weil, A.B., 2010, Quantifying vertical axis rotation in curved orogens: Correlating multiple data sets with a refined weighted least squares strike test: Tectonics, TC3012, v. 29, doi:10.1029/2008TC002312.

Zijderveld, J.D.A., 1967, A.C. demagnetization of rocks: Analysis of results, *in* Collinson, D.W., Creer, K.M., and Runcorn, S.K., eds., Methods in Palaeomagnetism: Amsterdam, Netherlands, Elsevier, p. 254–286.

MANUSCRIPT RECEIVED 23 MAY 2016
REVISED MANUSCRIPT RECEIVED 22 SEPTEMBER 2016
MANUSCRIPT ACCEPTED 03 NOVEMBER 2016

Printed in the USA